14. SITE 973[1]

Shipboard Scientific Party[2]

HOLE 973A

Date occupied: 27 April 1995

Date departed: 29 April 1995

Time on hole: 1 day, 20 hr, 30 min

Position: 35°46.820′N, 18°56.889′E

Bottom felt (drill-pipe measurement from rig floor, m): 3706.5

Distance between rig floor and sea level (m): 11.5

Water depth (drill-pipe measurement from sea level, m): 3695.0

Total depth (from rig floor, m): 3855.0

Penetration (m): 148.5

Number of cores (including cores having no recovery): 17

Total length of cored section (m): 148.5

Total core recovered (m): 86.8

Core recovery (%): 58.4

Oldest sediment cored:
Depth (mbsf): 148.50
Nature: clayey calcareous siltstone
Earliest age: early Pliocene

HOLE 973B

Date occupied: 27 April 1995

Date departed: 27 April 1995

Time on hole: 05 hr, 15 min

Position: 35°46.813′N, 18°56.889′E

Bottom felt (drill-pipe measurement from rig floor, m): 3710.0

Distance between rig floor and sea level (m): 11.5

Water depth (drill-pipe measurement from sea level, m): 3698.5

Total depth (from rig floor, m): 3719.5

Penetration (m): 9.5

Number of cores (including cores having no recovery): 1

Total length of cored section (m): 9.5

Total core recovered (m): 9.6

Core recovery (%): 101.3

Oldest sediment cored:
Depth (mbsf): 9.50
Nature: nannofossil ooze
Earliest age: Pleistocene

HOLE 973C

Date occupied: 29 April 1995

Date departed: 29 April 1995

Time on hole: 08 hr, 45 min

Position: 35°46.822′N, 18°56.889′E

Bottom felt (drill-pipe measurement from rig floor, m): 3707.0

Distance between rig floor and sea level (m): 11.6

Water depth (drill-pipe measurement from sea level, m): 3695.4

Total depth (from rig floor, m): 3716.5

Penetration (m): 9.5

Number of cores (including cores having no recovery): 1

Total length of cored section (m): 9.5

Total core recovered (m): 9.7

Core recovery (%): 102.2

Oldest sediment cored:
Depth (mbsf): 9.50
Nature: nannofossil clay
Earliest age: Pleistocene

HOLE 973D

Date occupied: 29 April 1995

Date departed: 1 May 1995

Time on hole: 1 day, 05 hr, 45 min

Position: 35°46.821′N, 18°56.892′E

Bottom felt (drill-pipe measurement from rig floor, m): 3705.6

Distance between rig floor and sea level (m): 11.6

Water depth (drill-pipe measurement from sea level, m): 3694.0

Total depth (from rig floor, m): 3858.2

Penetration (m): 152.6

Number of cores (including cores having no recovery): 9

Total length of cored section (m): 75.0

Total core recovered (m): 64.1

Core recovery (%): 85.5

Oldest sediment cored:
Depth (mbsf): 152.60
Nature: gypsiferous silty clay

HOLE 973E

Date occupied: 1 May 1995

Date departed: 1 May 1995

Time on hole: 13 hr

[1]Emeis, K.-C., Robertson, A.H.F., Richter, C., et al., 1996. *Proc. ODP, Init. Repts.*, 160: College Station, TX (Ocean Drilling Program).

[2]Shipboard Scientific Party is given in the list preceding the Table of Contents.

Position: 35°46.822′N, 18°56.881′E

Bottom felt (drill-pipe measurement from rig floor, m): 3705.6

Distance between rig floor and sea level (m): 11.8

Water depth (drill-pipe measurement from sea level, m): 3693.8

Total depth (from rig floor, m): 3737.6

Penetration (m): 32.0

Number of cores (including cores having no recovery): 2

Total length of cored section (m): 19.0

Total core recovered (m): 19.8

Core recovery (%): 104.2

Oldest sediment cored:
Depth (mbsf): 32.00
Nature: nannofossil clay
Earliest age: Pleistocene

Principal results: The main aims of drilling Site 973 on the toe of the Mediterranean Ridge known as the Hellenic accretionary wedge were largely achieved despite operational difficulties and a shortage of time at the end of the leg. The main results of importance in this section of early Pliocene to Holocene age concern evidence of increased levels of strain toward the base of the section (>100 mbsf) and the presence of an unusual and interesting geochemical environment related to upward geochemical mobility from assumed Messinian evaporates beneath.

The upper 84 m of the section is dominated by nannofossil ooze and nannofossil clay with sapropels and minor ash. Numerous intercalations of fine- to medium-bedded turbidites are present, including one approximately 14 m thick. The underlying section down to 146 mbsf comprises red-colored clayey nannofossil ooze overlying a calcareous silty claystone, with a diagenetically altered sapropel and veins of diagenetic gypsum.

Although the section is mainly nearly horizontally bedded, some intervals dip generally to the south and southwest. There is a small number of mainly steeply inclined normal faults. The diagenetic gypsum was deformed by several generations of shear-related effects, including tension gashes, en echelon fractures, and brecciation.

Pore-water analyses reveal downward increases in a number of parameters, including salinity, chloride, calcium, bromide, and magnesium. Sodium is an exception, and this may relate to the presence of a sodium-poor brine beneath. The pore-water data are dominated by upward diffusion and even advection of a late-stage brine with a magnesium-, sulfate-, and bromide-rich composition. This effect has dominated diagenetic reactions in the sedimentary column, especially where gypsum precipitation is taking place.

In conclusion, Site 973 provided interesting insights into the tectonic and geochemical processes operating in the lower toe of the Mediterranean Ridge accretionary wedge.

BACKGROUND AND OBJECTIVES

Site 973 is the second of two sites on the toe of the Mediterranean Ridge accretionary wedge. This second site is located slightly higher on the slope, at a water depth of 3700 m (Fig. 1). The objectives were identical to those of drilling at Site 972, as follows:

1. To investigate the structure of the Pliocene-Pleistocene section in relation to the large-scale processes of subduction and accretion operating in the distal part of the Mediterranean accretionary wedge;
2. To use the evidence of small-scale structures in the cores (i.e., faults and debris flows) to shed light on the vertical tectonic history in relation to accretionary processes and to determine if stresses related to subduction and accretion are transmitted into the overlying plate;

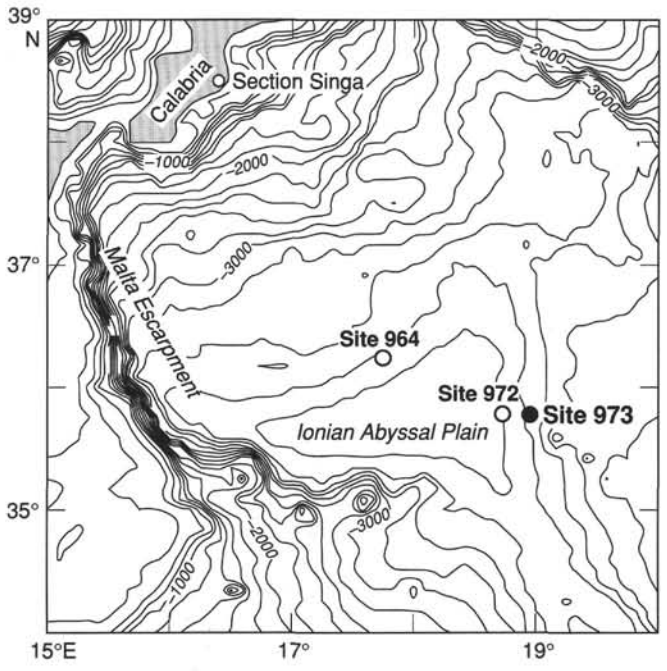

Figure 1. Location of Site 973 on the Outer Deformation Front of the Mediterranean accretionary wedge. Note the location of companion Site 972, slightly lower on the slope, and that of Site 964 farther northwest.

3. To make comparisons with the tectonic-sedimentary history of Site 972, which is located slightly lower on the toe of the accretionary wedge, in particular whether there is observable diachronism in tectonic processes;
4. To draw comparisons with the toe area of other accretionary wedge settings drilled during Leg 160, specifically the adjacent Calabrian accretionary wedge drilled at Site 964 on the Pisano Plateau and the lower Cyprus slope drilled at Site 968; and
5. To recover what we hoped would be an intact Pliocene-Pleistocene section of sapropels that could be compared with Sites 964 and 972.

GEOLOGICAL SETTING

Site 973 is located on the lower part of the Mediterranean Ridge accretionary wedge, slightly farther upslope than Site 972. The regional tectonic setting is as reviewed for Site 972 (see "Geological Setting" section, "Site 972" chapter, this volume). The site is located on a topographically rough area, and consists of a Pliocene-Pleistocene section that is presumed underlain by Messinian evaporite (see "Site Geophysics," section, this chapter).

One additional point of note is that the lower slope of the accretionary wedge in the vicinity of Sites 973 and 972 has a highly uneven topography. This contrasts with the area directly to the north, as shown in Figure 2, where the lower slope is much smoother. One possible reason for this difference relates to the nature of the Ionian (Messina) Abyssal Plain just beyond the active deformation front. In this region two distinct features are known, the Nathalie structure and the Victor Hensen structure. The southeastern of these two structures, the Victor Hensen Seahill, has an extent of approximately 60 km beneath the seafloor, from which it rises above the seafloor to a maximum elevation of 340 m, where recent dredging has shown that it includes Messinian facies (M. Cita, pers. comm., 1995). By contrast, the adjacent Nathalie structure is entirely beneath the seafloor. The two structures are separated by a strong reflector interpreted as the Messinian "M" reflector. Hirschleber et al. (1994) interpreted the

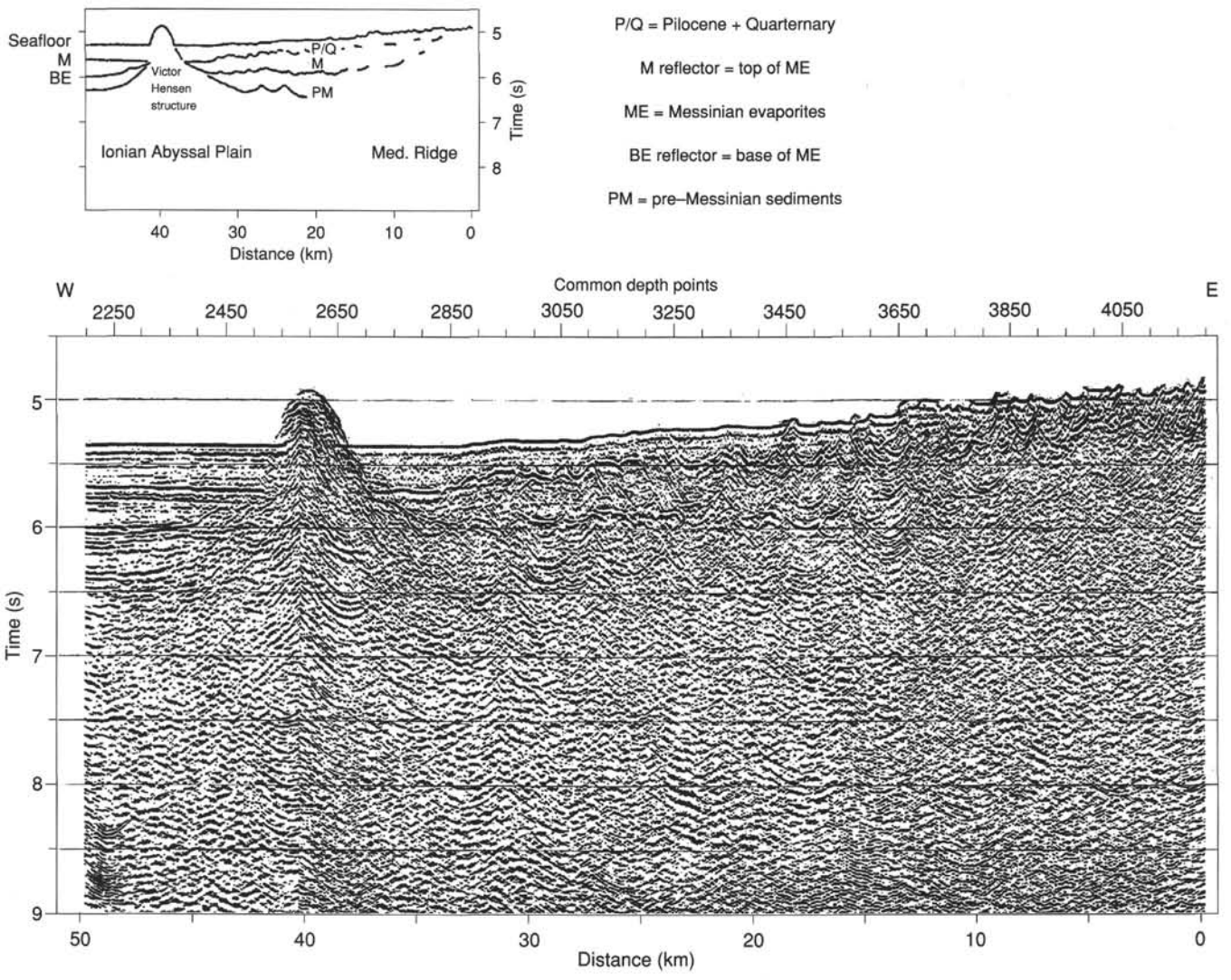

Figure 2. Single-channel seismic profile across the deformation front between the Ionian (Messina) Abyssal Plain and the Mediterranean Ridge. This east-west profile to the north of the Victor Hensen structure is where the incoming plate is free of major topographic irregularities, in contrast to Sites 972 and 973. The angle of dip of the downgoing slab can be seen. Inset: line interpretation (from Hirschleber et al., 1994).

Victor Hensen and Nathalie structures as the result of extensional tectonics in the Miocene that also controlled the deposition of intervening evaporites. More importantly, they concluded that these structures were later partly overlain by Pliocene-Pleistocene sediments.

The relevance of these observations is that the markedly irregular nature of the bathymetry of the deformation front drilled at Sites 973 and 972 could relate to the effect of subduction of a topographically irregular slab in the past, similar to the Victor Hensen and Nathalie structures. Such subduction could induce strong faulting and deformation of the toe of the wedge. It was hoped to test this hypothesis by comparative drilling of Sites 973 and 972. However, it was recognized that the décollement is located at much greater depths and could not be penetrated by our drilling.

OPERATIONS

Transit to Site 973

The ship was moved 11.4 nmi in dynamic-positioning mode while the pipe was pulled. The BHA cleared the rotary table at 0600 hr on 27 April.

Hole 973A

A Datasonics 354M beacon (S/N 1248, 14.5 kHz) was deployed at 0938 hr on 27 April. A full core barrel was obtained on the first APC core attempt and initially discarded; however, it was archived later as Hole 973B. Hole 973A (proposed Site MR-3) was spudded at 1300 hr on 27 April. The estimated seafloor was at 3695.0 m by drill-pipe measurement (DPM). APC Cores 160-973A-1H through 7H were taken to 65.0 mbsf (Table 1), with 66.70 m recovered (100.3% recovery). Orientation measurements were taken from Core 160-973A-3H. XCB Cores 160-973A-8X through 16X were taken from 65.0 to 146.5 mbsf. The bit was balling, and the rate of penetration was slow. The XCB shoes were plugging and five of the nine shoes jammed in stiff clay. The XCB shoe broke off on Core 160-973A-17X, junking the hole and terminating coring. The spacer sub was nearly cut by a loose bit cone, indicating bit failure. The 11 $^{7}/_{16}$-in. bit had lost the number 2 cone and had severe shirttail abrasion wear.

Hole 973B

A Datasonics 354M beacon (S/N 1248, 14.5 kHz) was deployed at 0938 hr on 27 April. The first APC core attempt was from 3710 m

Table 1. Coring summary for Site 973.

Core	Date (1995)	Time (UTC)	Depth (mbsf)	Length cored (m)	Length recovered (m)	Recovery (%)
160-973A-						
1H	27 April	1345	0.0–8.0	8.0	7.95	99.4
2H	27 April	1440	8.0–17.5	9.5	9.92	104.0
3H	27 April	1545	17.5–27.0	9.5	9.34	98.3
4H	27 April	1650	27.0–36.5	9.5	9.27	97.6
5H	27 April	1815	36.5–46.0	9.5	9.67	102.0
6H	27 April	1930	46.0–55.5	9.5	10.21	107.5
7H	27 April	2100	55.5–65.0	9.5	8.87	93.3
8X	27 April	2340	65.0–74.5	9.5	5.36	56.4
9X	28 April	0135	74.5–84.1	9.6	0.88	9.2
10X	28 April	0330	84.1–93.7	9.6	0.00	0.0
11X	28 April	0545	93.7–103.3	9.6	0.00	0.0
12X	28 April	0545	103.3–112.9	9.6	0.02	0.2
13X	28 April	0940	112.9–122.5	9.6	3.59	37.4
14X	28 April	1315	122.5–132.1	9.6	9.05	94.3
15X	28 April	1720	132.1–141.7	9.6	1.11	11.5
16X	28 April	2120	141.7–146.5	4.8	1.54	32.1
17X	29 April	0050	146.5–148.5	2.0	0.00	0.0
Coring totals:				148.5	86.8	58.4
160-973B-						
1H	27 April	1300	0.0–9.5	9.5	9.61	101.3
Coring totals:				9.5	9.61	101.3
160-973C-						
1H	29 April	1810	0.0–9.5	9.5	9.71	102.2
Coring totals:				9.5	9.71	102.2
160-973D-						
1H	29 April	1925	0.0–8.9	8.9	8.88	99.8
2H	29 April	2025	8.9–14.9	6.0	5.99	99.8
3H	29 April	2305	14.9–24.4	9.5	8.14	85.7
4H	30 April	0005	24.4–33.9	9.5	10.02	105.5
5H	30 April	0100	33.9–43.4	9.5	9.15	96.3
6H	30 April	0150	43.4–52.9	9.5	9.99	105.0
7H	30 April	0310	52.9–62.4	9.5	9.97	105.0
8X	30 April	1225	140.0–144.9	4.9	0.98	20.0
9X	30 April	1630	144.9–152.6	7.7	1.01	13.1
Coring totals:				75.0	64.1	85.5
160-973E-						
1H	1 May	0140	13.0–22.5	9.5	9.95	105.0
2H	1 May	0310	22.5–32.0	9.5	9.86	104.0
Coring totals:				19.0	19.8	104.2

below rig floor (mbrf) and 9.62 m was recovered. The core was not considered to be a valid mud-line core and was not archived initially; however, it was sectioned for demonstration purposes later, and sapropels were discovered and sampled. The core was archived as Hole 973B, but left on the ship. For the record, Hole 973B was spudded at 1415 hr on 27 April. APC Core 160-973B-1H was taken from 0 to 9.5 mbsf (Table 1), with 9.62 m recovered (101.3% recovery). The seafloor depth (3698.5 m) and the location are the same as for Hole 973A. The bit cleared the seafloor at Hole 973B at 1500 hr on 27 April.

Hole 973C

The ship was moved 10 m to the north. Hole 973C was spudded at 1810 hr on 29 April. The first mud-line core recovered only 1 m, and was discarded as a water core. The second core was shot at 3695.4 m, and recovered a full barrel, which was archived. A seafloor depth of 3695.4 m by DPM was indicated. APC Core 160-973C-1H was taken to 9.5 mbsf with 9.73 m recovered (102.2% recovery).

Hole 973D

The ship was not moved. The first mud-line core was shot at 3694 mbrf and recovered 8.88 m. Hole 973D was spudded at 1900 hr on 29 April. APC Cores 160-973C-1H through 7H were taken from 0 to 62.4 mbsf, with 62.14 m recovered (99.6% recovery). Four of the seven cores were partial strokes in clay and sand, and four of the seven liners imploded or burst and had to be pumped out.

The hole was drilled with a center bit from 62.4 to 140.0 mbsf in 5.5 rotating hr. XCB Cores 160-973-8X and 9X were taken from 140.0 to 152.6 mbsf, with 12.6 m cored and 1.99 m recovered (15.8% recovery). The rate of penetration was slow. The XCB shoes were jammed in stiff clay. A hole-cleaning sweep was circulated on the last core.

Logging Operations at Hole 973D

Coring was terminated owing to time constraints, a go-devil was pumped, and the bit was pulled to 71.5 mbsf (without a conditioning trip) for a short logging program. An induction/sonic log was run to 3858.2 mbrf total depth (no fill) in 4.66 hr. Time was not available to run another log, so the bit was pulled and cleared the seafloor at 0155 hr on 1 May.

Hole 973E

Additional cores were needed to cover a coring gap at about 17.5 mbsf. The ship was not moved. Hole 973E was spudded at 0240 hr on 1 May. The seafloor depth was 3694.1 mbrf. The 117/16-in. hole was washed from 0 to 13.0 mbsf. APC Cores 160-973E-1H and 2H were taken from 13.0 to 32.0 mbsf, with 19.8 m recovered (104.2% recovery). The bit cleared the seafloor at 0525 hr on 1 May. The coring wire lines were coated with Compound L and the drill pipe was inhibited with Coat 405. The bit cleared the rotary table at 1700 hr on 1 May.

SITE GEOPHYSICS

Site 973 is located on a small hill (water depth 3604 m, uncorrected) about 20 km to the east of Site 972 (see Fig. 3, "Site 972" chapter, this volume). The small-scale relief of the seafloor is on the order of 25 to 75 m, as at Site 972, and the resulting diffractions obscure most deeper reflections (Fig. 3). The seafloor is slightly more disturbed than at Site 972 to the west, reflecting the more advanced deformation expected farther up the accretionary prism. One flatter area of ponded sediments to the east is almost 1 km wide at a depth of about 3632 m. The section of almost continuous diffractions to the west suggests a more disturbed zone. Some discontinuous stronger reflectors appear to shallow to the west from 5.4 s two-way traveltime (TWT) at the eastern end of the seismic line to 5.2 s TWT 1 or 2 km to the west of the site, giving the impression that the disturbed zone to the west may overlie the toe of a westward-directed thrust and might therefore represent associated folding and reverse faulting. Apart from these differences with Site 972, the geology of Site 973 appears to be similar to that of the neighboring site to the west (see "Site Geophysics" section, "Site 972" chapter, this volume).

LITHOSTRATIGRAPHY

The sedimentary sequence recovered at Site 973 consists of an 84-m-thick late Pliocene to Holocene age section of nannofossil ooze and nannofossil clay, with intercalated sapropels. This sequence contains interbeds of sands, silts, and nannofossil clays, which are generally of a decimeter to meter scale but include one 14-m-thick interval of sand grading upward to nannofossil clay (Unit I). These sediments are separated by a zone of no recovery from a sequence of lower to upper Pliocene, red-colored, clayey nannofossil ooze and an underlying calcareous silty claystone with a relict sapropel that is veined and partly replaced by gypsum. The lithostratigraphic summary for Holes 973A, 973C, 973D, and 973E is shown in Figure 4.

Criteria employed in lithostratigraphic description and classification at Site 973 included (1) visual observation of color; (2) visual observation of sedimentary structures, including bioturbation; (3)

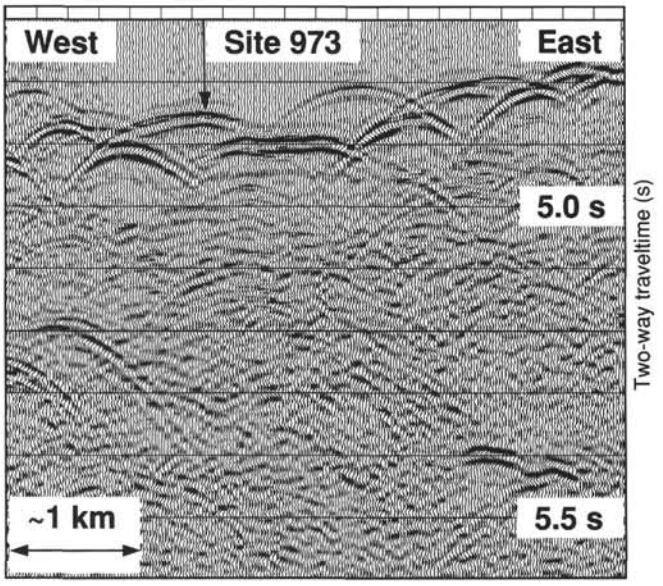

Figure 3. Seismic profile across Site 973. Traces are about 25 m apart.

smear-slide examination; (4) color reflectance spectrophotometry measurements; and (5) carbonate and organic carbon determinations.

Color Reflectance

Color scanning was performed at 2-cm intervals. The color intensity provided an excellent record of the occurrence of both sapropels and the thicker turbidite beds. The color record was used to aid interhole correlation and compile a composite section (see "Composite Depths" section, this chapter). Detailed color reflectance studies (Fig. 5) show a consistent trend of upward-decreasing red chroma beneath sapropels (particularly oxidized sapropels). Also evident are the characteristic flat signatures of the sand beds.

Description of Lithostratigraphic Units

Lithostratigraphic Unit I

Description: Nannofossil ooze, clayey nannofossil ooze, sands, silts, clays, and mixed sediments
Intervals: Cores 160-973A-1H through 9X, 160-973B-1H, 160-973C-1H, 160-973D-1H through 7H, and 160-973E-1H and 2H
Depth: 0–84.1 mbsf, Hole 973A; 0–9.5 mbsf, Hole 973B; 0–9.5 mbsf, Hole 973C; 0–62.4 mbsf, Hole 973D; 13–32 mbsf, Hole 973E
Age: late Pliocene to Holocene

Lithostratigraphic Unit I is a combination of pelagic sediments consisting of nannofossil ooze, clayey nannofossil ooze, and sapropels which are interbedded with sands, silts, clays, and mixed sediments. These interbeds are commonly graded by grain size and/or color and may be correlated among the holes. The variety of types that may be recognized is listed below. The composition of the dominant lithology, according to smear-slide analysis, is most commonly nannofossil ooze and varies from about 50% to 90% nannofossils, 2% to 15% foraminifers, and 5% to 50% clay. The topmost 10 m contains a higher proportion of clay, which decreases downcore. Localized centimeter- to decimeter-scale layers of foraminifer nannofossil ooze occur sporadically throughout the sequence.

Most of the interbeds within the sequence are decimeter, or at most meter, scale in thickness. However, an interval that grades from clayey sand through nannofossil silty clay to nannofossil clay and clayey nannofossil ooze occurs between 48.7 and 64.4 mbsf (Hole 973A). This interval appears virtually structureless, apart from a 30-cm-thick layer at 56.8 mbsf that appears to contain evidence of bioturbation. In the absence of bedding features, and from the evidence of overall grading, this layer might, however, be regarded as the deposit of a single depositional event.

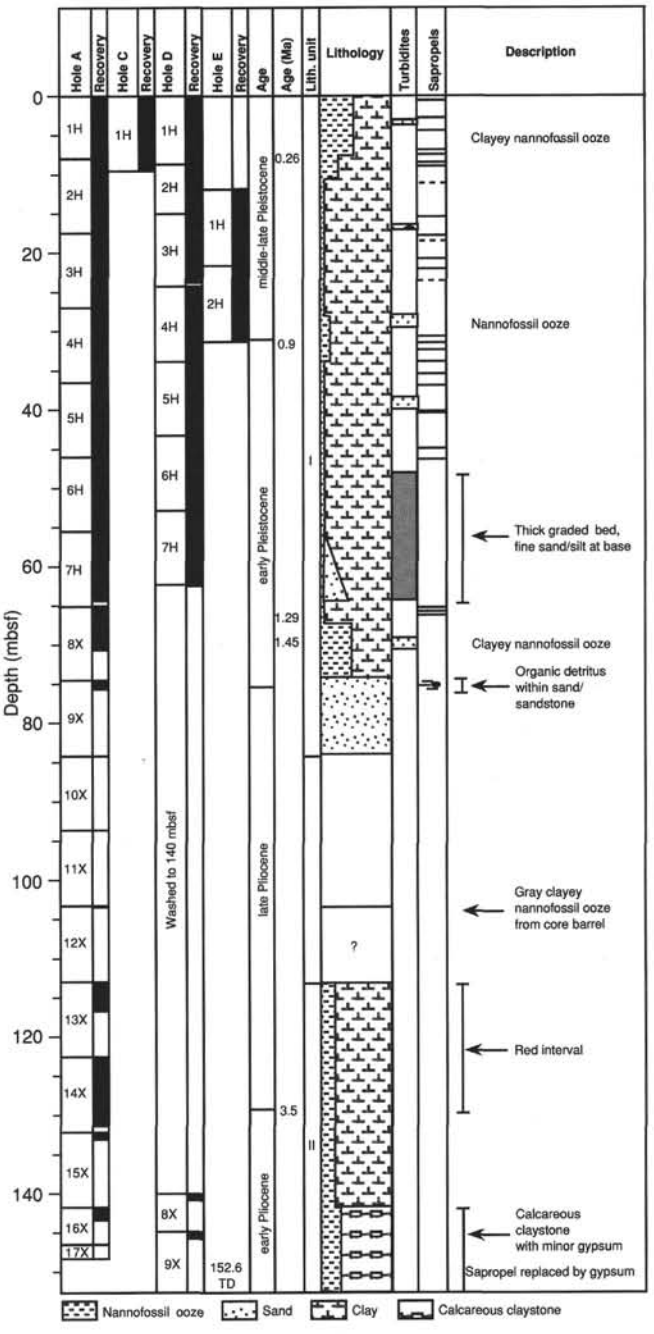

Figure 4. Core recovery, age information, and lithostratigraphic summary for Holes 973A, 973C, 973D, and 973E.

The lowest recovered sediments in Unit I are clayey carbonate sand and sandstone, composed dominantly of redeposited micritic limestone fragments and foraminifers. The sandstone shows parallel lamination and contains black organic fragments (see "Organic Geochemistry" section, this chapter) (Fig. 6).

Ash

Three thin (<3 cm) ash layers occur in the upper part of the section. Volcanic glass is also a minor component of the dominant lithol-

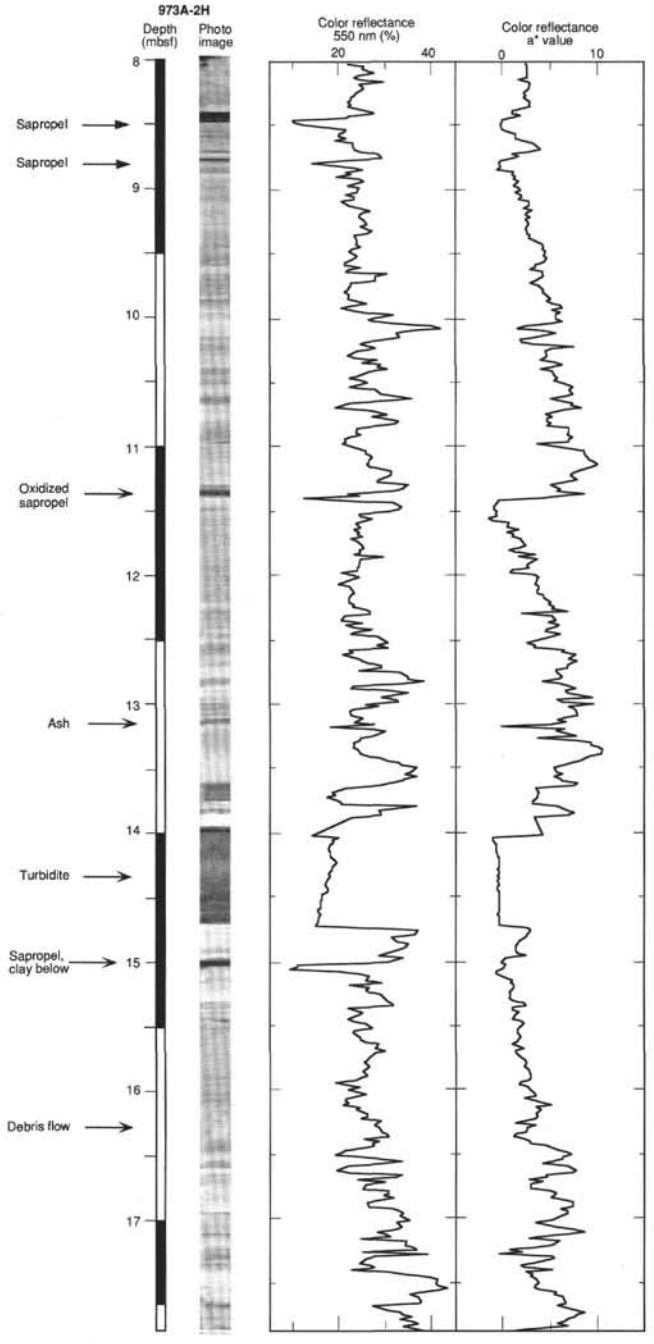

Figure 5. Plot of color data for Core 160-973A-2H showing, from left to right: depth and lithologic occurrences, scanned photographic image of the core, and color reflectance at 550 nm (general brightness) and a*, for which higher values indicate increasing redness. Note the thin sapropels marked by troughs in brightness and the dark flat tone from the turbidite. A progressive decrease in redness occurs beneath the sapropels.

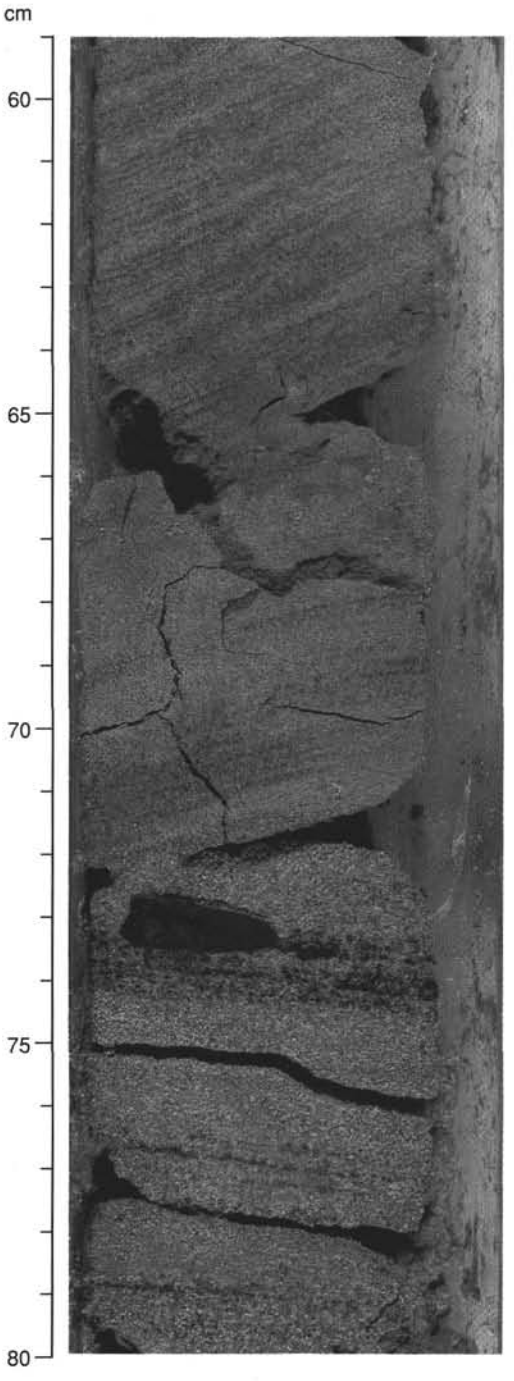

Figure 6. A semilithified, parallel-laminated sandstone containing redeposited organic fragments (Section 160-973A-9X-1, 59–80 cm).

ogies, where it probably represents ash layers redistributed and intermixed by bioturbation.

Sand, Silt, and Clay Interbeds

Several different types of interbeds interrupt the nannofossil clay/sapropel sequence. The most common of these are ~1- to 10-cm-thick beds of yellowish brown (10YR 5/4) nannofossil clay (31% $CaCO_3$), which commonly show color and compositional grading to the dominant lithology of light gray (10YR 7/2) nannofossil ooze (64% $CaCO_3$) (Fig. 7). These nannofossil clay interbeds are common between 0 and 48 mbsf and locally form more than 50% of the section over 1-m intervals (e.g., Sections 160-973A-2H-2 and 2H-3, 100 cm, through 2H-4, 65 cm).

A 63-cm-thick bed of graded, light brownish gray (10YR 7/2) carbonate sand and silt with a prominent erosive base occurs at 3.8 mbsf (Hole 973A), and a 1.45-m-thick bed of similar composition is at 27.45 mbsf (Hole 973A). These beds are characterized by a high proportion of micritic rock fragments, 16%–20% quartz, 23%–40% rock fragments, 16%–30% foraminifers, and 2%–5% mica. Thinner examples of this bed type occur interbedded with the sequence.

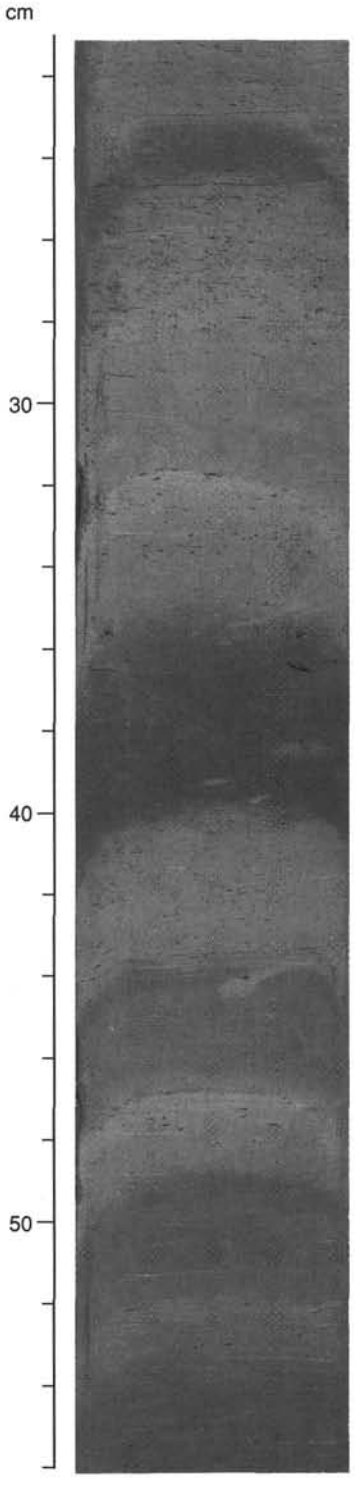

Figure 7. A series of 1- to 5-cm-thick beds of yellowish brown (10YR 5/4) nannofossil clay (31% $CaCO_3$, Sample 160-973A-2H-4, 38–39 cm), which commonly show color and compositional grading to the dominant lithology of light gray (10YR 7/2) nannofossil ooze or foraminifer nannofossil ooze (64% $CaCO_3$, Sample 160-973A-2H-4, 41–42 cm). The dark, submillimeter specks (e.g., from 25 to 28 cm) are foraminifers within the "background" sediments (Section 160-973A-2H-4, 21–56 cm).

Rare, dark greenish gray (5GY 4/1) to dark gray (5Y 4/1), quartz-rich, graded sand-silt beds occur at 4.58 mbsf (11 cm thick) and 14.74 mbsf (72 cm thick). These beds contain quartz (40%) with rock fragments (mainly carbonate, 20%), and foraminifers (20%), and mica (5%).

Examples of very rare, but distinctively colored, pale olive (5Y 6/3) beds of nannofossil clay, with parallel silt laminae in the basal part, occur at 20.45 mbsf (15 cm thick) and 27.98 mbsf (17 cm thick).

Evidence for Erosion

There is extensive evidence for erosion of pelagic sediments beneath the interbeds of sand, particularly below contacts with the light brownish gray or gray carbonate sands. Several of these beds exhibit irregular bases (Fig. 8A), and one bed shows evidence of undercutting of the subjacent nannofossil ooze (Fig. 8B). A sand bed is in erosive contact with the top bed of a distinctive tripartite sapropel at 48.59 mbsf in Hole 973D (Fig. 9A). By contrast, in Hole 973A, the upper bed of the correlative sapropel has been entirely eroded (Fig. 9B). Evidence for more substantial erosion of sapropels is contained in a bed at 40.5 mbsf (Hole 973A). This graded silty clay has a dark gray color similar to an underlying sapropel and contains both organic matter and pyrite, which were probably eroded and redeposited from a sapropel (Fig. 10).

Sapropels

More than 27 sapropels were recovered from the upper Pleistocene through Holocene section at Site 973. Compositionally, from smear-slide analysis, the sapropels generally resemble the surrounding dominant lithology but contain, in addition, organic matter and pyrite. The thicker sapropels occur in two main packets, from 0 to 9 mbsf and between 31 and 41.5 mbsf (Hole 973A).

The upper group of sapropels contains several of the typical upper Pleistocene sequence (*sensu* McCoy, 1974) with S1, S5, and S6 all present. They are generally dark gray (5Y 4/1), dark olive gray (5Y 3/2), or very dark gray (5Y 3/1) in color. A very thin (1 cm), partially oxidized sapropel at 2.94 mbsf (Hole 973A; 2.37 mbsf, Hole 973B) may correspond to S2(?), not hitherto recorded during Leg 160 (Fig. 11). Some sapropels appear to be missing from the sequence, including possibly S3 and S4. Their absence may be the result of erosion by the currents responsible for deposition of the interbeds. Some sapropels (e.g., S5) are interrupted by silt and mud interbeds (Fig. 12). Among the upper packet of sapropels, only S6 (Fig. 13) and the sapropel about 1 m below appear to be macroscopically laminated.

Reddish brown sediments without sapropels were deposited in the intervals 22.1–30.8 mbsf (Hole 973A) and 22.5–32 mbsf (Hole 973D) during the early part of the middle-late Pleistocene. In the lower group of sapropels of early Pleistocene age, individual beds attain organic carbon levels as high as 17% (Fig. 14) (see "Organic Geochemistry" section, this chapter) with a more normal range of 2%–10%.

Lithostratigraphic Unit II

Description: Clayey nannofossil ooze
Intervals: Cores 160-973A-13X through 16X and 160-973D-8X and 9X
Depth: 102.83–146.5 mbsf, Hole 973A; 140–152.6 mbsf, Hole 973D
Age: early-late Pliocene

The sediments of Unit II between 113 and 142 mbsf are composed of color-banded, reddish brown (5YR 5/4) to white (10YR 8/2), clayey nannofossil ooze. This sediment is extensively veined with gypsum, which infills both subvertical and bed-parallel veins (Fig. 15) (see "Structural Geology" section, this chapter).

The sediments in the last core to have recovery (160-973A-16X) consist of clayey calcareous siltstone and claystone that are heavily veined with gypsum and also contain localized disseminated gypsum

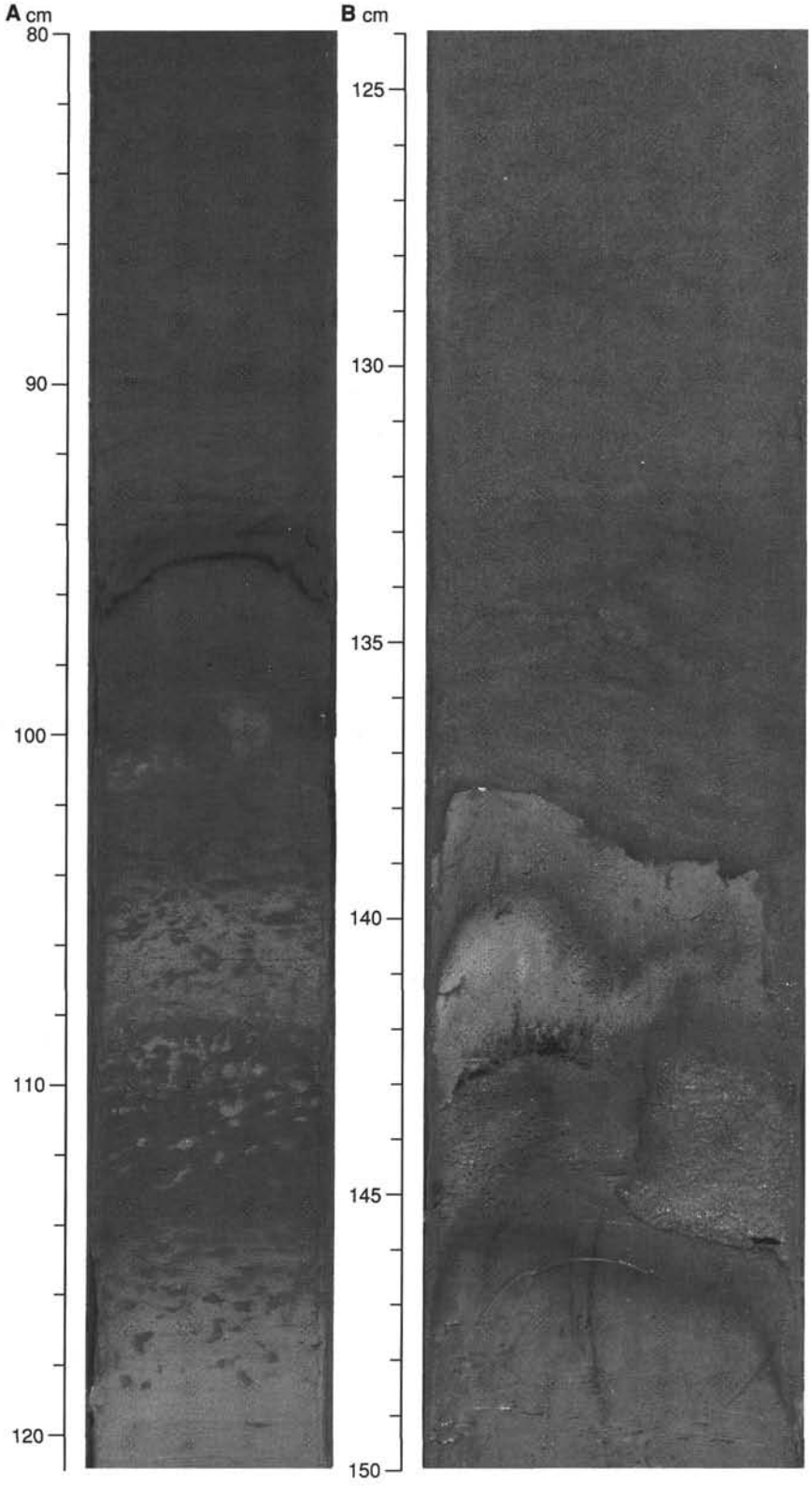

Figure 8. Evidence for erosion beneath sand beds. **A.** The jagged, irregular, erosive base to a carbonate sand bed cuts into interbedded light gray nannofossil ooze and yellowish brown nannofossil clay (Section 160-973A-4H-2, 80–121 cm). **B.** Undercut nannofossil ooze at the base of a bed of gray carbonate sand (Section 160-973D-4H-4, 124–150 cm).

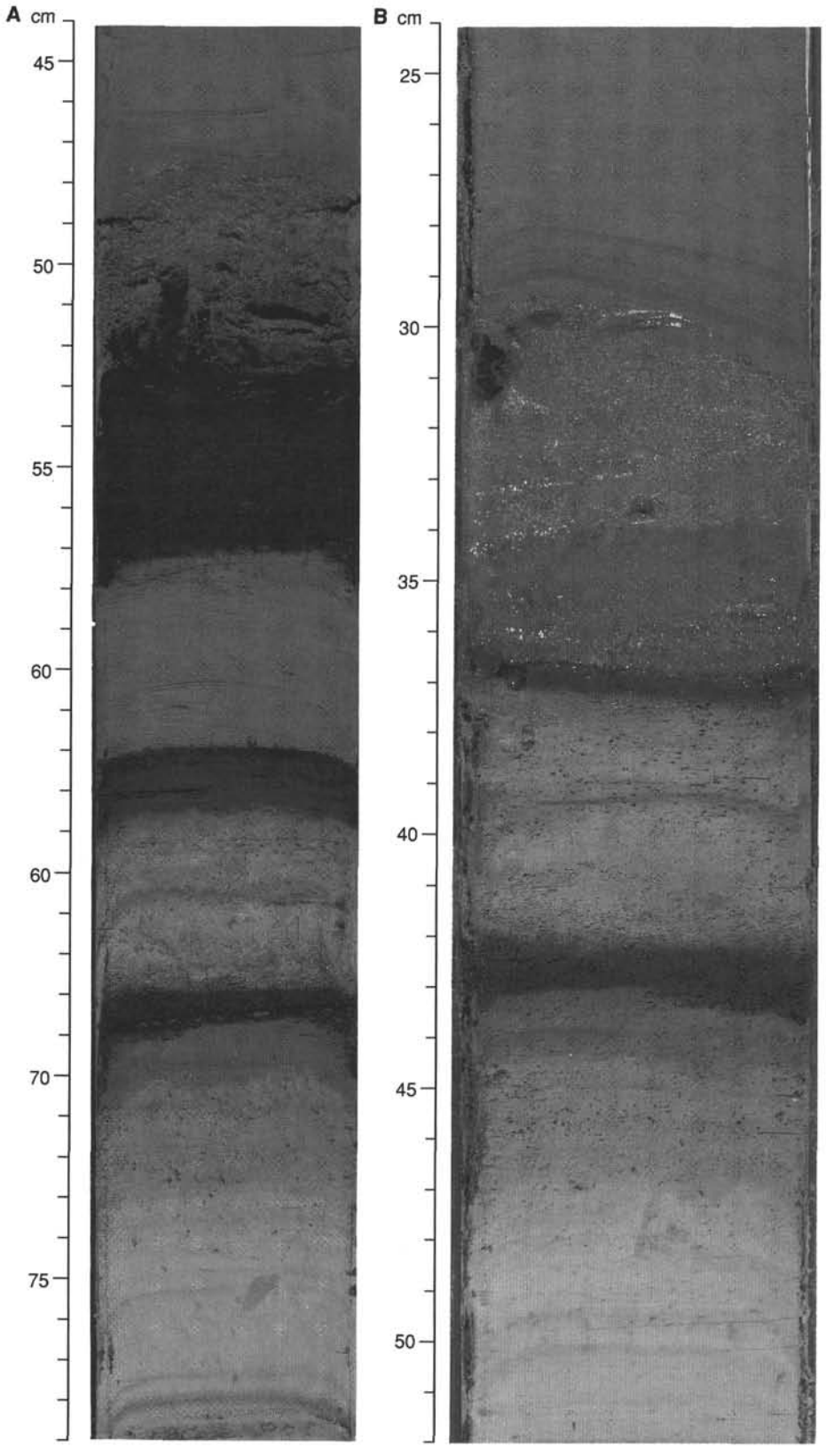

Figure 9. Differential erosion beneath a sand/mud turbidite observed in different holes. **A.** A bed of sand lies on the eroded top of a tripartite sapropel (Section 160-973D-6H-4, 44–79 cm). **B.** A bed of sand displays an erosive contact with the middle bed of the equivalent sapropel and shows evidence for 10 cm of differential erosion between the two holes (Section 160-973A-6H-1, 24–52 cm).

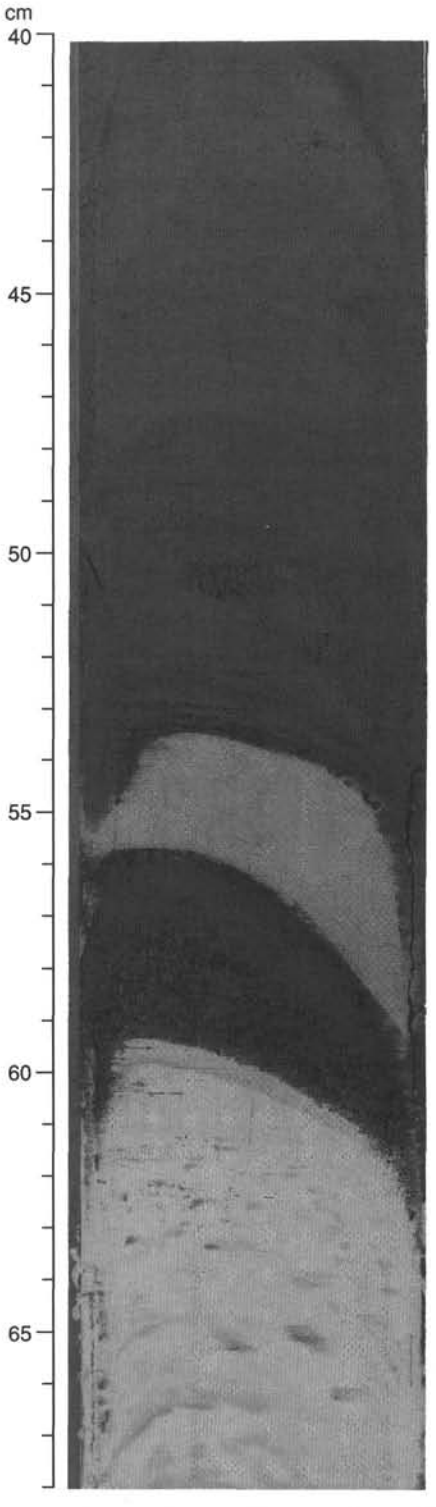

Figure 10. A sapropel above pale nannofossil ooze is overlain by a 2-cm-thick bed of nannofossil clay, which is succeeded by a dark gray, graded silty clay containing fragments of organic matter and pyrite, probably derived from erosion of a sapropel (Section 160-973A-5H-3, 40–68 cm).

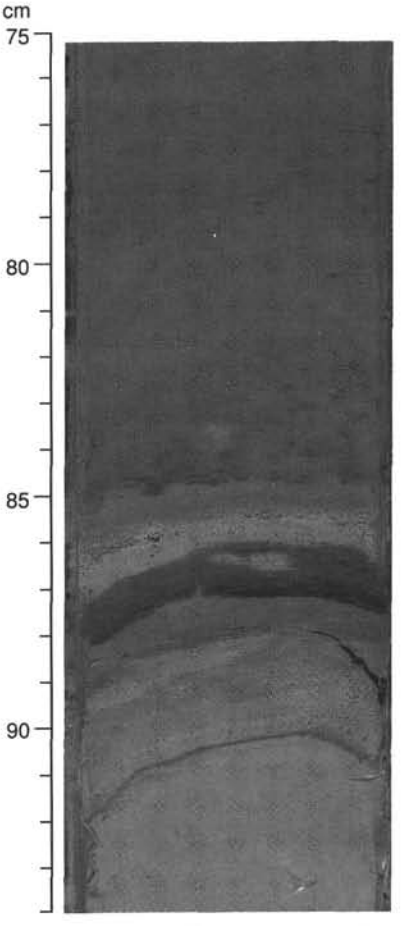

Figure 11. This thin sapropel, unusually oxidized in its lower part, may correspond to S2 (Section 160-973C-1H-2, 75–94 cm).

crystals. A black (5Y 2.5/1) bed consisting almost entirely of euhedral gypsum crystals was observed, from smear-slide analysis, to contain minor quantities of brownish to black organic matter(?) (Fig. 16). It is suggested that this black bed may represent an original sapropel now almost completely replaced by gypsum cement. No nannofossils occur in this core. The presence of some disseminated gypsum crystals, in addition to the veining, suggests that the carbonate fraction may have been recrystallized by the same solutions that precipitated the gypsum, thus destroying the calcareous microfossils.

Interhole Correlation and Development of a Composite Section

In order to provide a stratigraphic correlation among the holes at Site 973, distinctive lithologic markers were identified in all holes. The sedimentological characteristics and position of each sapropel and each major turbidite bed were recorded, as were the position and composition of the more distinctive ash layers. A check on the visual correlation was provided by color-scanner data (see "Color Reflectance" above); reference was also made to selected MST data including magnetic susceptibility.

Discrepancies in the number of sapropels recovered in the various holes can be attributed to (1) the presence of gaps in coring between successive cores (see "Composite Depths" section, this chapter) and (2) erosion and removal of some sapropels, probably by the currents responsible for deposition of the sand beds.

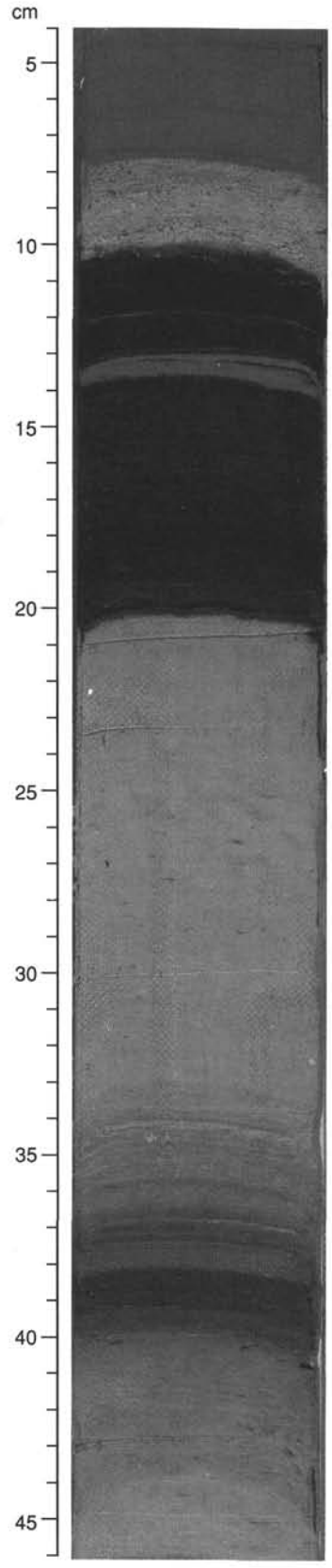

Figure 12. Sapropel S5 is interrupted by two interbeds, a lower 17-cm-thick graded silty clay and an upper thin (4 mm thick) mud (Section 160-973A-1H-4, 4–46 cm).

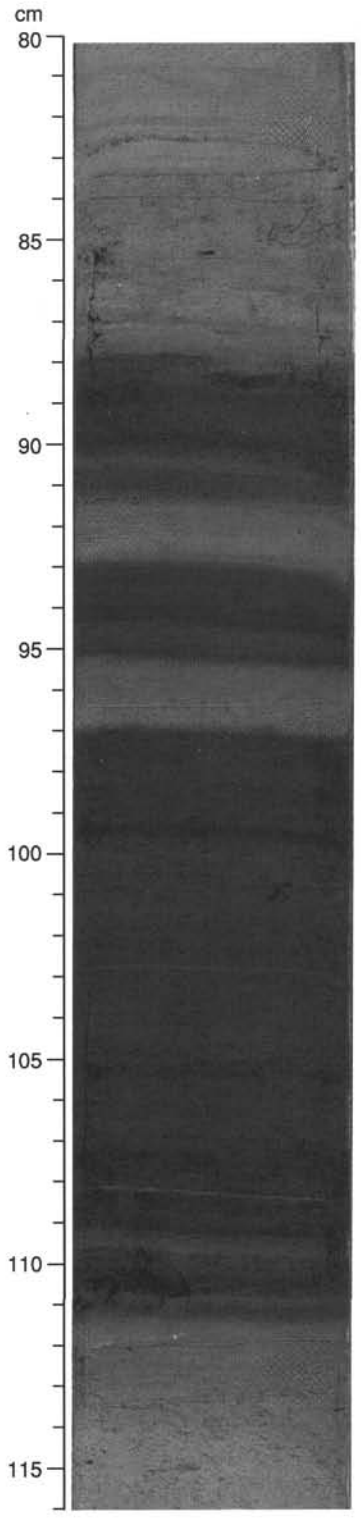

Figure 13. Sapropel S6 is laminated and contains the two typical distinctive nannofossil ooze intercalations (Section 160-973A-1H-5, 80–116 cm).

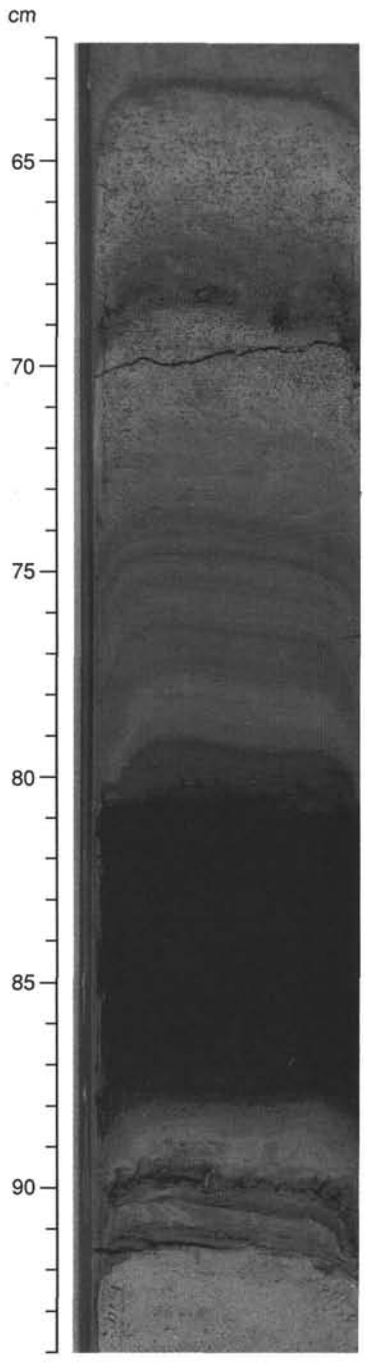

Figure 14. An example of an organic-rich (17% TOC) lower Pleistocene sapropel showing color banding and foraminifer-rich layers (speckled) above (Section 160-973A-4H-5, 62–94 cm).

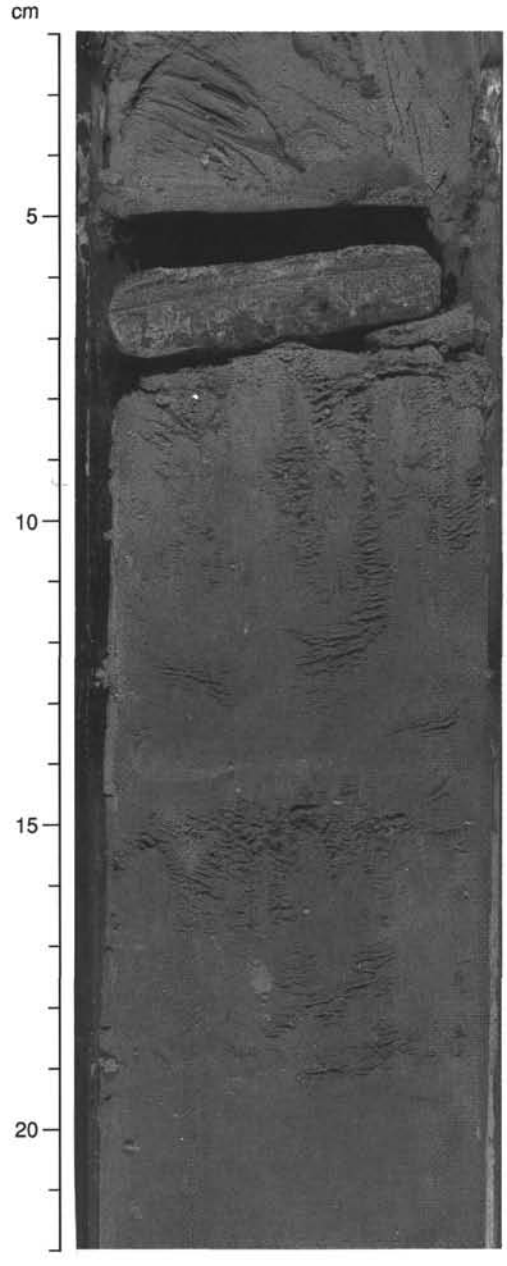

Figure 15. An interval of clayey nannofossil ooze with a thin layer (probably of vein origin) of gypsum (Section 160-973A-14X-1, 2–22 cm).

A complete list of all sapropels recovered at Site 973 is shown in Table 2, and the stratigraphic correlation, taken as far as was possible from shipboard work, is presented in Figure 17. From the five holes cored, a composite section/sampling route was constructed using the most intact sequences from Holes 973A, 973D, and 973E (see Table 6, "Composite Depths" section, this chapter, and Fig. 17).

Depositional History

The earliest deposition recorded at Site 973 is the sedimentation of nannofossil clay, of probable early Pliocene age, containing sapropels (Core 160-973A-16X). This was succeeded by an interval of lower to upper Pliocene red-colored clayey nannofossil ooze, which may correlate with similar intervals in other Leg 160 sites, such as Site 969. The upper Pliocene section was poorly recovered, but the Pliocene-Pleistocene sediments are clayey carbonate sand and sandstone, composed dominantly of redeposited micritic limestone fragments and foraminifers. The poor recovery in the upper Pliocene interval at 84–113 mbsf may result from the presence of sands similar to those that are, in part, cemented as sandstone between 60 and 74.5 mbsf (Hole 973D). However, the uranium peaks recorded in the downhole logs (see "Downhole Measurements" section, this chapter) are typical of the signature of sapropels in other holes and suggest that sapropels may be interbedded with the sands. Pleistocene sedimentation continued with intermittent deposition and preservation of organic-rich sediment as sapropels against a background of nannofossil ooze interrupted by the deposits of turbidity currents, some of

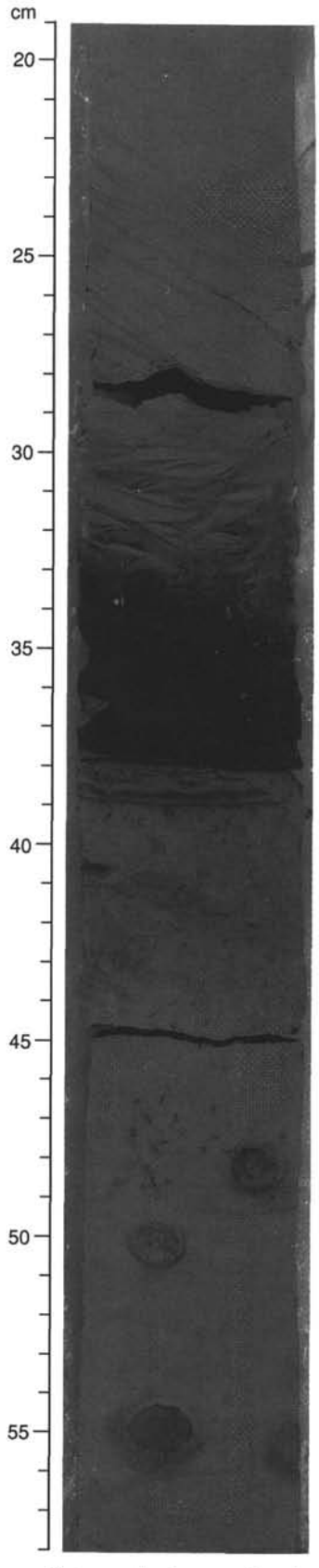

Figure 16. Calcareous siltstone and calcareous silty claystone with a relict sapropel now replaced by gypsum. Note the prominent veins of gypsum above the sapropel (Section 160-973A-16X-1, 19–58 cm).

which were strongly erosive. The composition of the sands records erosion of a carbonate sequence composed of foraminiferal lime mudstones. No sapropels were deposited in the early part of the middle-late Pleistocene time interval, during which time consistently reddish brown oxidized sediments accumulated in common with the other, deeper Leg 160 sites (967, 969, and 964).

BIOSTRATIGRAPHY AND SEDIMENTATION RATES

Calcareous Nannofossils

Calcareous nannofossils were studied primarily from core-catcher samples from Hole 973A. To provide a higher resolution biostratigraphy, additional samples were collected from within each core where a zonal boundary was believed to exist. Though some turbidites were observed in the cores (see "Lithostratigraphy" section, this chapter), all nannofossil zones from the late-middle Pleistocene through the upper part of the early Pliocene were recognized (Fig. 18).

Hole 973A

Samples 160-973A-1H, 23 cm, through 1H-CC, are in Zone MNN21a and contain *Emiliania huxleyi* in quantities lower than those of the acme zone, which was not identified upsection. The accompanying assemblage includes small *Gephyrocapsa* (<3.5 µm), *Gephyrocapsa oceanica* s.l., *Helicosphaera kamptneri, Coccolithus pelagicus, Rhabdosphaera clavigera,* and *Pontosphaera japonica.* Reworked species fluctuate from rare to few and consist of late Pleistocene, Pliocene, and Late Cretaceous age taxa.

Samples 160-973A-2H-1, 115 cm, and 2H-3, 113 cm, were placed into Zone MNN20, which is a gap zone defined by the absence of both *E. huxleyi* and *Pseudoemiliania lacunosa.* The accompanying in situ and reworked assemblages are similar to those found uphole.

Samples 160-973A-2H-5, 133 cm, through 4H-4, 17 cm, contain nannofossils from Zone MNN19f. The upper boundary of the zone is defined by the last occurrence of *P. lacunosa,* whereas the lower boundary is defined by the first occurrence of *Gephyrocapsa* sp. 3. The placement of the upper boundary of this zone is difficult because the abundance of *P. lacunosa* is rare to few in samples uphole. The interpretation of where the top of the zone exists is subjective and based solely on the consistent occurrence of *P. lacunosa* below Sample 160-973A-2H-1, 115 cm. The uphole occurrences are interpreted to be reworked, whereas the samples herein are considered in situ. The in situ and reworked assemblages that accompany *P. lacunosa* are similar to those found uphole. *Gephyrocapsa* sp. 3 is present in Samples 160-973A-3H-1, 126 cm, through 4H-4, 17 cm.

Samples 160-973A-4H-6, 28 cm, and 4H-CC, contain nannofossils from Zone MNN19e. This interval was interpreted as a gap zone identified by the absence of *Gephyrocapsa* sp. 3 and large *Gephyrocapsa* (>5.5 µm). Small *Gephyrocapsa* and *P. lacunosa* dominate the assemblage.

Samples 160-973A-5H-1, 58 cm, through 8X-1, 28 cm, contain varying quantities of large *Gephyrocapsa* (>5.5 µm), which mark Zone MNN19d. The accompanying assemblage is dominated by *G. oceanica* s.l., small *Gephyrocapsa,* and *P. lacunosa.*

Samples 160-973A-8X-1, 119 cm, through 8X-3, 110 cm, contain nannofossils from Zone MNN19c. This zone is a gap zone defined by the absence of both *Calcidiscus macintyrei* and large *Gephyrocapsa* (>5.5 µm). Small *Gephyrocapsa* and *G. oceanica* s.l. dominate the assemblage. *P. lacunosa* and *Helicosphaera sellii* are common.

Samples 160-973A-8X-4, 30 cm, through 9X-1, 22 cm, contain nannofossils from Zone MNN19b. This zone is identified by the presence of both *G. oceanica* s.l. and *C. macintyrei.* The accompanying in situ and reworked assemblages are similar to those found uphole.

Table 2. Position and organic carbon content of sapropels recovered from Hole 973A and correlatable beds in Holes 973C, 973D, and 973E.

Core, section, interval base (cm)	Depth (mbsf)	Thickness (cm)	C_{org} (%)	Number	Comments	Core, section, interval base (cm)	Depth (mbsf)	Thickness (cm)	Comments
160-973A-						160-973C-			
1H-1, 66	0.66	6		S1					
1H-2, 144	2.94	1				1H-2, 87	2.37	2	Oxidized
1H-4, 20	4.7	10	13.41	S5		1H-3, 121	4.21	10	
1H-5, 110.5	7.105	23.5	3.37	S6		1H-5, 74	6.74	23	
1H-6, 3.5	7.535	4	4.73			1H-5, 119	7.19	4	
						1H-6, 24	7.74	14	
						1H-6, 63	8.13	5	
2H-1, 50	8.5	5	2.32						
2H-1, 80	8.8	1							
2H-3, 41	11.41	6			Oxidized				
2H-5, 106	15.06	4	2.1						
3H-1, 31	17.81	1			Oxidized				
3H-1, 119	18.69	5			Oxidized				
3H-3, 127	20.9	2							
3H-4, 102	22.15	4							
3H-5, 126	23.89	13			Oxidized				
4H-3, 86	30.86	3							
4H-3, 95.5	30.955	2	17.27						
4H-4, 21	31.71	1	5.54						
4H-4, 102	32.52	1							
4H-4, 114	32.64	6	4.08						
4H-5, 88	33.88	7	17.23						
4H-6, 120	35.7	6	5.85						
5H-1, 62	37.12	2	7.73						
5H-3, 60	40.1	>10	4.69		Base of turbidite-reworked sapropel				
5H-4, 31	40.65	7							
5H-7, 50	44.4	10			Oxidized sapropel?				
5H-7, 105	44.95	1							
6H-1, 38	46.38	1			Top eroded				
6H-1, 44	46.44	1							
8X-1, 28	65.28	1.5	9.29						
8X-1, 80	65.8	8	7.07						
8X-1, 123	66.23	3.5	18.53						
9X-1, 73	75.23				Dark clast				
16X-1, 38	142.08	5			Gypsum replacing sapropel?				

Sample 160-973A-9X-CC contains a nannofossil assemblage in which both *G. oceanica* s.l. and *Discoaster brouweri* are absent and includes small *Gephyrocapsa, P. lacunosa, C. macintyrei,* and *Helicosphaera sellii.* Core 160-973A-10X had no recovery; however, a small amount of mud was collected from the teeth of the core catcher and analyzed. Although the location of the sediment scraped from the core catcher can not be determined, the assemblage is similar to that of the preceding core. Based on the assemblage, these intervals were placed into uppermost Pliocene Zone MNN19a.

Below Core 160-973A-10X the biostratigraphy is problematic owing to poor core recovery. Core 160-973A-11X was empty and Core 160-973A-12X contained only a few centimeters of gray mud. The sample from Section 160-973A-12X-CC contains *C. macintyrei, D. brouweri, Discoaster surculus, Discoaster intercalaris,* and *P. lacunosa.* Despite the presence of *D. surculus,* this sample was placed into Zone MNN18.

Samples 160-973A-13X-1, 62 cm, through 14X-1, 53 cm, contain *Discoaster tamalis* and an accompanying assemblage that includes *D. brouweri, Discoaster pentaradiatus,* and *D. surculus.* Samples 160-973A-14X-2, 137 cm, and 14X-4, 63 cm, may be included in Zone MNN16a, but the nannofossils are so diluted by carbonate fragments that the placement of this sample into a zonation is not possible.

Samples 160-973A-14X-5, 20 cm, through 15X-1, 13 cm, contain *Reticulofenestra pseudoumbilicus* and thus belong to Zone MNN14–15. The accompanying assemblage is similar to that found in the preceding zone.

The recovered sediments below Sample 160-973A-15X-1, 13 cm, cannot be confidently placed into a zonation, owing to paucity of nannofossils. Samples from Core 160-973A-16X are barren of nannofossils.

Planktonic Foraminifers

A sedimentary sequence spanning the Pleistocene through the lower Pliocene was recovered in Hole 973A (Fig. 18). Planktonic foraminiferal assemblages were analyzed from core-catcher samples. Further stratigraphic refinement was provided through analyses of additional samples from within each core.

Pleistocene planktonic foraminifers are generally common to abundant and consist of well-diversified and moderately to well-preserved faunas. By contrast, Pliocene assemblages are generally less diverse and moderately to poorly preserved. At the bottom of the sequence, planktonic foraminifers are generally rare and some samples are completely barren.

The *Truncorotalia truncatulinoides excelsa–Globigerina cariacoensis* interval is identified from Samples 160-973A-1H-CC through 9X-CC. Planktonic foraminiferal assemblages are relatively uniform throughout the Pleistocene sequence. Representative taxa include *Orbulina universa, Globorotalia inflata, Globigerinoides ruber, Globorotalia scitula, Globigerina bulloides, Turborotalita quinqueloba, Globigerinita glutinata, Globigerinita juvenilis,* and *Neogloboquadrina pachyderma* (both dextral and sinistral forms). Rare taxa include *Globigerinoides sacculifer, Pulleniatina obliquiloculata, Globigerinoides gomitulus, Globigerinoides pyramidalis, Globigerinoides conglobatus,* and *Hastigerinopsis riedeli.*

Reworking affects the Pleistocene sediments throughout. Evidence of this was found in Sample 160-973A-7H-CC, where shallow-water benthic foraminifers (e.g., *Planorbulina mediterranensis* and *Elphidium* spp.) occur with deep-water species (e.g., *Articulina tubulosa*). Sample 160-973A-9X-CC also contains a few specimens of *Sphaeroidinellopsis* spp. displaying a different degree of preservation than the accompanying assemblage.

Table 2 (continued).

Core, section, interval base (cm)	Depth (mbsf)	Thickness (cm)	Comments	Core, section, interval base (cm)	Depth (mbsf)	Thickness (cm)
160-973D-				160-973E-		
1H-1, 94	0.94	3		1H-2, 75.5	15.25	3
1H-1, 82	5.32	12		1H-4, 51	18.01	1
1H-1, 101	5.51	2		1H-6, 143	21.93	1
1H-6, 27	7.77	24				
1H-6, 70.5	8.205	5				
1H-CC, 16	8.75	16				
2H-1, 11	9.01	1	Oxidized			
3H-1, 114	16.04	2				
3H-4, 23	19.63	2				
3H-5, 13	21.03	5				
4H-6, 24	32.14	3				
4H-6, 36	32.26	3				
4H-6, 116	33.06	2				
4H-7, 53	33.93	1	Part of doublet			
4H-7, 64	34.04	6.5	Part of doublet			
5H-2, 64	36.04	12	Drilling disturbed			
5H-4, 36	38.52	3				
5H-CC, 15	42.55	15				
6H-2, 103	45.93	3				
6H-4, 57	48.47	5	Part of triplet			
6H-4, 63	48.53	1	Part of triplet			
6H-4, 69	48.59	1	Part of triplet			
6H-5, 74	50.14	7	Oxidized			

No sediment was recovered in Cores 160-973A-10X and 11X. Sample 160-973A-12X-CC contains the Pliocene species *Globigerinoides obliquus* and in the absence of *G. inflata* and *Globorotalia bononiensis* was tentatively assigned to the MPL5a–5b interval.

Samples 160-973A-13X-CC through 14X-4, 18–20 cm, were placed in Zone MPL4a, based on the co-occurrence of *Sphaeroidinellopsis* spp. and *Globorotalia puncticulata.* Zone MPL4b, defined by the presence of *Sphaeroidinellopsis* spp. in the absence of *G. puncticulata,* may be missing in Hole 973A. In this interval, residues are also characterized by abundant gypsum crystals (see "Lithostratigraphy" section, this chapter).

Zone MPL3 was recognized by the presence of *Globorotalia margaritae* in Sample 160-973A-14X-6, 100–102 cm. The sediments below contain a few nondiagnostic Pliocene species or are devoid of planktonic foraminifers.

Sedimentation Rates

Sedimentation rates for Hole 973A were calculated solely on calcareous nannofossil events (Table 3). Owing to poor core recovery and sediment quality, the foraminiferal datums probably do not reflect the true last and first occurrences for this hole. The data are plotted on an age vs. depth curve, shown in Figure 19. An error line is shown on the figure to indicate the degree of uncertainty as to the location of the nannofossil events within the hole.

Calculated sedimentation rates vary from 23 to 111 m/m.y. from the top of the hole through the cored sequence. Six significant shifts in sedimentation rates were observed. From the seafloor to the first occurrence of *Gephyrocapsa* sp. 3, sedimentation rates averaged 33 m/m.y. From the first occurrence of *Gephyrocapsa* sp. 3 to the last occurrence of *Gephyrocapsa* (>5.5 µm) sedimentation rates decreased to 23 m/m.y. Sedimentation rates then increased significantly to the maximum value of 111 m/m.y. between the last occurrence and the first occurrence of large *Gephyrocapsa* >5.5 µm. Between the latter datum and the first occurrence of *G. oceanica* s.l., sedimentation rates decreased to an average of 38 m/m.y.

PALEOMAGNETISM

Site 973 is in a sedimentary environment similar to Site 972, but with fewer turbidites (see "Lithostratigraphy" section, this chapter). Therefore, Site 973 is better suited for paleomagnetic studies than Site 972, although it is far from ideal. Paleomagnetic measurements made on archive halves of each core section at 10-cm intervals after AF demagnetization at 25 mT were restricted to the upper 70 m of Hole 973A (i.e., to the bottom of Core 160-973A-8X). NRM intensities were well above the noise level of the magnetometer throughout the measured interval in Hole 973A (Fig. 20). Many of the intensity peaks coincide with sapropels, as discussed by Roberts et al. (this volume). The amplitude of the variations in the NRM intensity and the magnetic susceptibility records are different, with much of the susceptibility record showing larger amplitude variations than the intensity record. These differences may reflect stratigraphic variations in the input of magnetic grains, as well as postdepositional changes. The occurrence of numerous turbidites in Hole 973A (see "Lithostratigraphy" section, this chapter) provides a mechanism for transport and deposition of coarse magnetic grains that have high susceptibility and relatively low remanence intensity. Susceptibility peaks were not observed for all of the turbidites seen in the record, which may result from the deposition of different types of turbidites or from differences in source areas (see "Lithostratigraphy" section, this chapter).

Weak intensities and relatively low, and less varied, susceptibilities are in the interval from 48.65 to 65 mbsf (Fig. 20). This interval contains a homogeneous gray mud that grades into a silty mud and

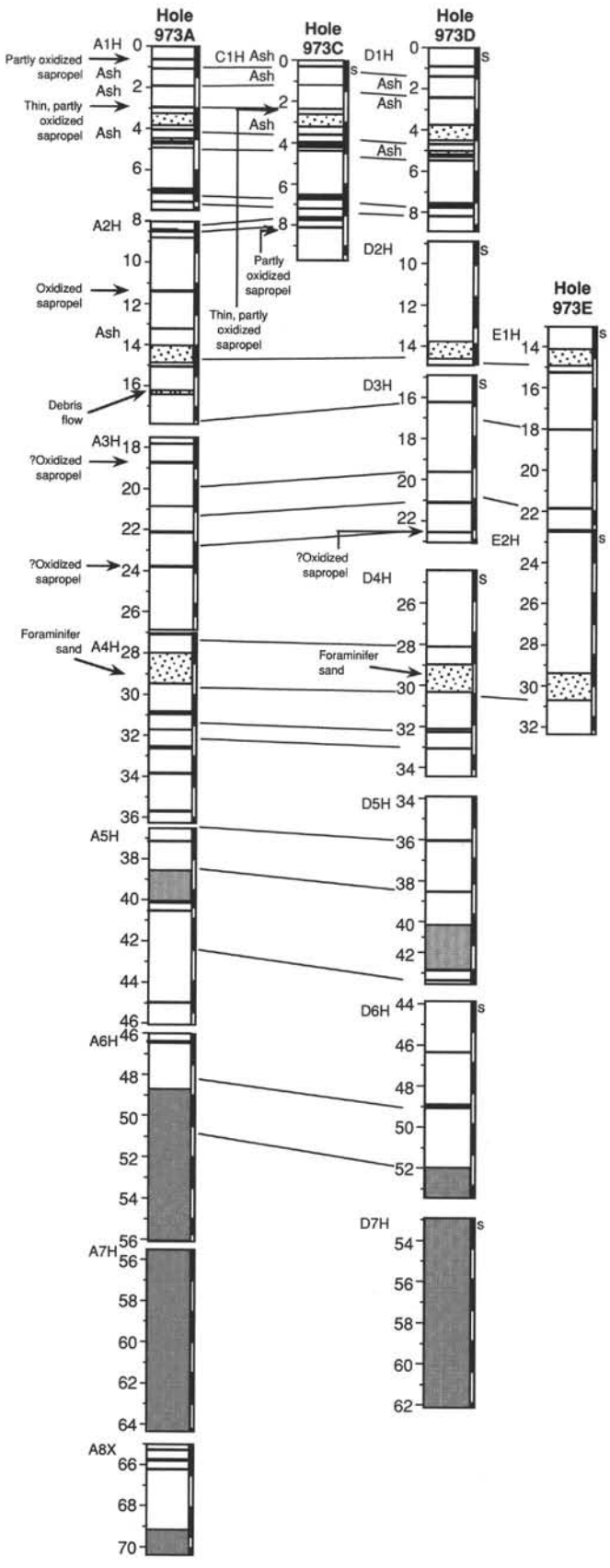

Figure 17. Summary of the occurrence of sapropels, ash layers, and the thicker sand beds (shaded) correlated among Holes 973A, 973C, 973D, and 973E.

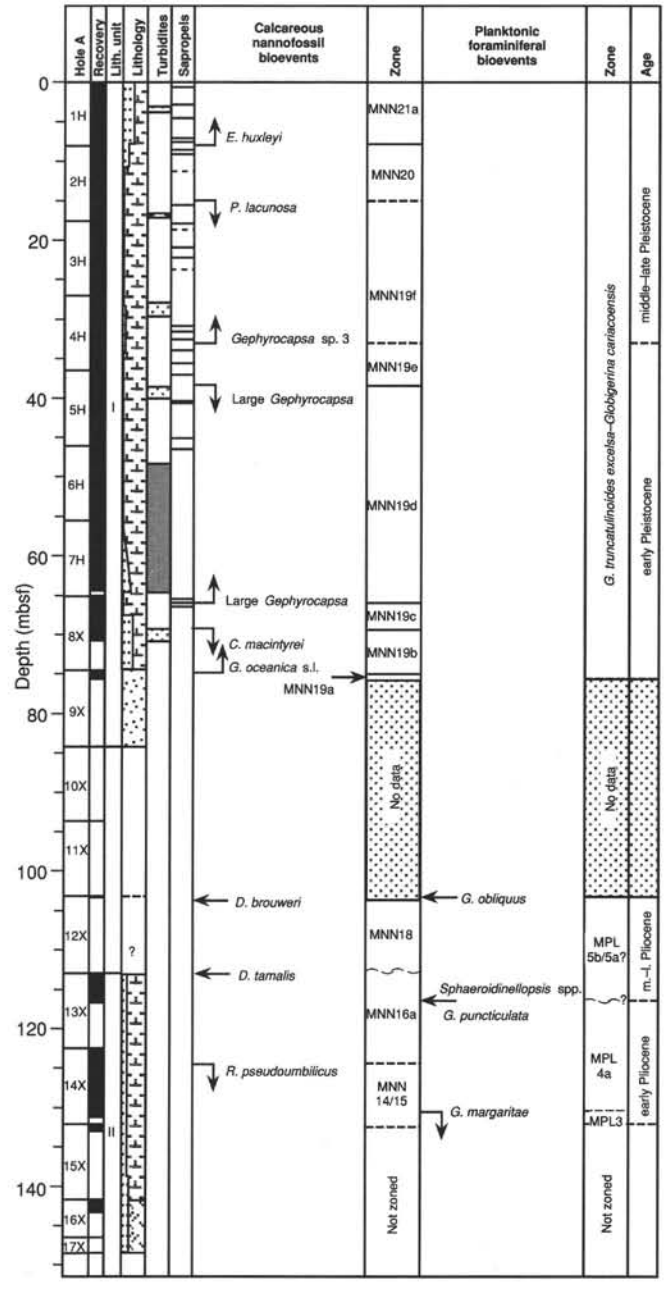

Figure 18. Composite of biostratigraphic events recognized in sediments recovered from Hole 973A including the lithostratigraphic record.

Table 3. Stratigraphic list of calcareous nannofossil and planktonic foraminifer events for Site 973.

Event	Core, section, interval (cm)	Depth (mbsf)	Age (Ma)
	160-973A-		
FO *E. huxleyi**	1H-CC	7.95	0.26
LO *P. lacunosa*	2H-5, 133	15.33	0.46
FO *Gephyrocapsa* sp. 3	4H-4, 17	31.67	0.99
LO *Gephyrocapsa* >5.5 µm	5H-1, 58	37.6	1.25
FO *Gephyrocapsa* >5.5 µm	8X-1, 28	65.28	1.5
LO *C. macintyrei*	8X-4, 30	69.8	1.62
FO *G. oceanica* s.l.	9X-1, 22	74.72	1.75

Notes: FO = first occurrence; LO = last occurrence; * = to be confirmed by scanning electron microscopy.

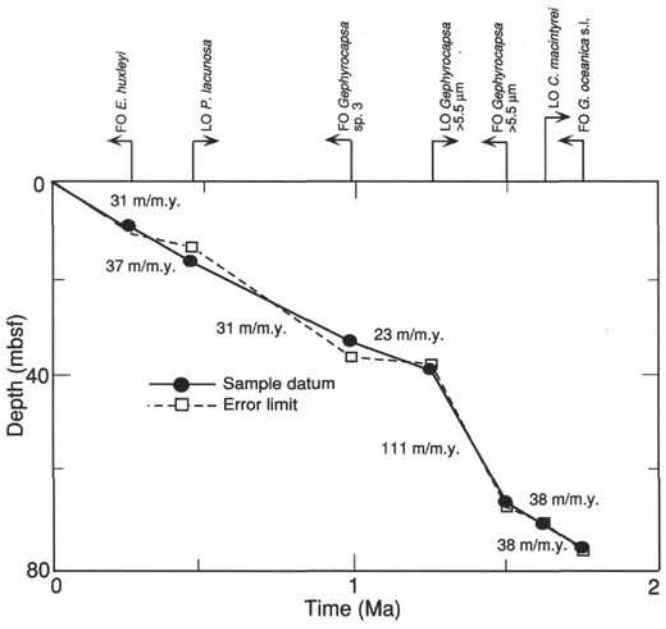

Figure 19. Age vs. depth diagram showing selected calcareous nannofossil and planktonic foraminifer datums with corresponding sedimentation rates. The line corresponds to the sample where the marker species was found for the corresponding first or last occurrence datum, and the dashed line corresponds to the nearest sample where the marker species was not found.

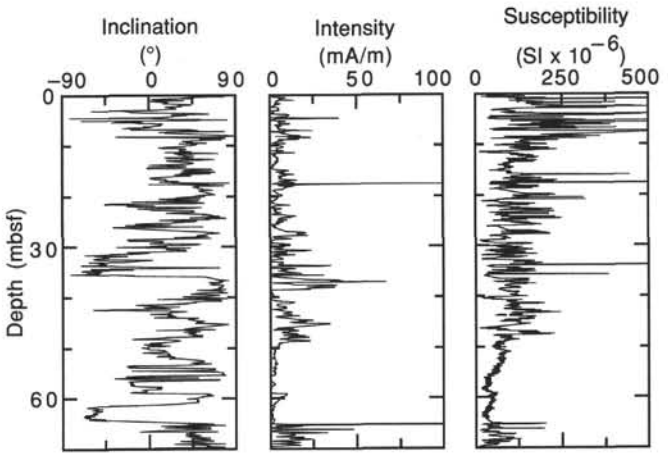

Figure 20. Paleomagnetic inclination, intensity, and magnetic susceptibility for Hole 973A. Inclination and intensity were measured after AF demagnetization at 25 mT.

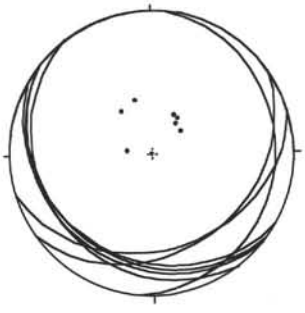

Figure 21. Equal-area lower hemisphere plot of the distribution of tilted bedding planes from Cores 160-973A-3H through 6H with respect to the geographic coordinates. Both poles and great circles are shown.

then into a sandy mud toward the base of the unit. The graded lower part of the unit is interpreted to represent a turbidite (see "Lithostratigraphy" section, this chapter). The relative uniformity of the lithology, compared with the rest of the sequence, accounts for the subdued intensity and susceptibility signals.

The whole-core inclination profile determined from Hole 973A is dominated by normal polarity (Fig. 20). The paleontological data indicate that the bottom of the sequence measured occurs within the lowermost Pleistocene, near the first occurrence of large *Gephyrocapsa* (see "Biostratigraphy and Sedimentation Rates" section, this chapter), which is dated at about 1.5 Ma in the Mediterranean area (Sprovieri, 1993). This suggests that almost 50% of the sediment should be characterized by reverse polarity and that the Matuyama/Brunhes boundary and the Jaramillo Subchron should be preserved in the record. This is not clearly evident in the whole-core record shown in Figure 20. Insufficient time was available to measure the number of discrete paleomagnetic samples necessary to elucidate the polarity stratigraphy at Site 973. The possibility of determining a useful magnetic polarity stratigraphy from Site 973 must therefore be evaluated after detailed post-cruise studies.

STRUCTURAL GEOLOGY

The holes drilled at Site 973 are located on the southern toe of the Mediterranean Ridge higher up the slope to the northeast of Site 972 (see "Site Geophysics" section, this chapter). Bedding measurements on Cores 160-973A-2H through 6H, which were recovered using oriented APC drilling, indicate that the beds broadly dip south to southwest (Fig. 21). Gypsum layers and veins were recovered in Cores 160-973A-16X and 160-973D-8X and 9X (see "Lithostratigraphy" section, this chapter).

Low- to moderately dipping beds (2°–32°) are visible in Cores 160-973A-2H, 3H, 5H, and 6H (Table 4). Cores 160-973A-3H through 6H were corrected to geographic coordinates using the Tensor tool data and plotted both as poles and great circles in Figure 21. The dominant direction of dip is toward the southwest. Bedding is mainly horizontal, both in the lower cores in Hole 973A (i.e., Cores 160-973A-8X through 17X) and throughout Hole 973D.

Normal faults with small offsets (0.1 to 1.2 cm) are visible in Core 160-973D-1H (Table 4). In three cases, these faults are associated with organic-rich layers. Because of the necessity of preserving intact sapropel sequences for post-cruise sampling, measurement of the second apparent dip was not possible. An indication of the minimum possible true dip of the faults can be gained from their moderate- to high-angle (26°–66°) apparent dip on the core face. All of the faults observed were traced by hairline to millimeter-scale veins of dark fine-grained material that vary in thickness along the length of the fault and some of which wedge out completely (e.g., Section 160-973D-1H-5, 57–61 cm). In Sections 160-973D-1H-5 and 1H-6, subvertical fault zones up to 44 cm in length were seen. These zones are also defined by dark narrow veins between which paler material, similar to the host sediment, occurs. Offsets are variable along the length of the feature.

Between 140 and 152.6 mbsf (Cores 160-973A-16X and 160-973D-8X and 9X), microveins and small-scale reverse faults were observed (Fig. 16, "Lithostratigraphy" section, this chapter). The veins are filled with fibrous gypsum and concentrated in particular areas (e.g., Sections 160-973A-16X-1, 20–30 cm, and 160-973D-9X-1, 0–20 cm). In some places, moderately dipping veins less than 1 mm wide are cut by similar, nearly perpendicular gypsum veins that offset the first generation with a reverse sense of movement (1–4

Table 4. Structural data collected at Site 973.

Core, section, interval (cm)	Depth (mbsf)	Feature	Offset width (cm)	Orientation on core face (degrees)[1]		Second apparent orientation (degrees)		Calculated orientation (degrees)		Geographic orientation (degrees)		Comments
				Apparent dip	Direction	Apparent dip	Direction	Dip	Direction	Dip	Direction	
160-973A-												
2H-5, 110	15.10	SB		0	90	2	180	2	180			Color change
2H-6, 40–41	15.90	SB		11	270	19	0	22	331			Ash
2H-6, 46–47	15.96	SB		8	270	14	0	16	331			Color change
3H-1, 105–107	18.55	SB		20	270	24	0	30	321	30	145.5	
3H-5, 31–32	22.94	SB		13	90	18	0	22	35	22	219.5	Ash
3H-5, 112–113	23.75	SB		12	90	24	0	26	26	26	210.5	
3H-5, 146–147	24.09	SB		14	90	21	0	25	33	25	217.5	
3H-6, 65	24.78	SB		12	270	30	0	32	339	32	163.5	
3H-7, 45–46	26.08	SB		16	90	14	0	21	49	21	233.5	Ash
5H-CC, 5	45.45	SB		0	90	0	0	0	0	0	3.5	
6H-1, 122–124	47.22	SB		14	270	0	180	14	270	14	276.5	Ash
16X-1, 2–6	141.72	V_1		41	270	9	0	41	280			Microvein, filled with gypsum
16X-1, 4–5	141.74	V_4		6	90	Not visible						Microvein, filled with gypsum
16X-1, 4–8	141.74	V_2		36	270	28	180	42	234			Microvein, filled with gypsum
16X-1, 5–6	141.75	V_5		36	90	19	180	39	115			Microvein, filled with gypsum
16X-1, 5–9	141.75	V_3		29	270	20	180	34	237			Microvein, filled with gypsum
16X-1, 7–14	141.77	V_6		70	270	0	19	71	289			Microvein, filled with gypsum
16X-1, 11	141.81	V_8		3	90	7	180	8	157			Microvein, filled with gypsum
16X-1, 11–16	141.81	V_7		38	270	21	180	41	244			Microvein, filled with gypsum
16X-1, 18–21	141.88	V_9		43	270	61	0	64	333			Microvein, filled with gypsum
16X-1, 19–23	141.89	V_{10}		30	270	Not visible						Microvein, filled with gypsum
16X-1, 21–24	141.91	V_{11}		21	270	27	180	33	217			Microvein, filled with gypsum
16X-1, 21–26	141.91	V_{12}		37	270	28	180	43	235			Microvein, filled with gypsum
16X-1, 22–27	141.92	V_{13}		28	270	25	180	35	229			Microvein, filled with gypsum
16X-1, 24–28	141.94	V_{18}		25	90	40	0	44	29			Microvein, filled with gypsum, 1 mm offset (top toward west with respect to the core liner)
16X-1, 24–28	141.94	V_{16}		25	270	29	180	36	220			Microvein, filled with gypsum
16X-1, 24–29	141.94	V_{15}		37	270	30	180	44	233			Microvein, filled with gypsum
16X-1, 26–31	141.96	V_{14}		34	270	34	180	44	225			Microvein, filled with gypsum
16X-1, 27–31	141.97	V_{17}		33	270	3	0	33	275			Microvein, filled with gypsum
16X-1, 28–31	141.98	V_{19}		24	90	2	0	24	86			Microvein, filled with gypsum, 1 mm offset (top toward west with respect to the core liner)
16X-1, 40–41	142.10	F		38	270	21	180	41	244			Microfault
160-973D-												
1H-4, 122–126	5.72	F	0.2	38	270							Normal
1H-4, 122–126	5.72	F	0.1	37	270							Normal
1H-5, 40–44	6.4	V		26	270							Wispy dark vein structures
1H-5, 40–44	6.4	V		51	270							Wispy dark vein structures
1H-5, 57–61	6.57	F	0.5	66	270							Tapering-upward wedge of gray mud with normal offset
1H-5, 73–82	6.73	F	1	56	270							Normal in sapropel
1H-5, 83–127	6.83	F	3	85-90	270							Subvertical zone 1.5 cm thick comprising dark gray mud veins with paler material between them; offsets are variable down the length of the zone, which is more diffuse at the base
1H-6, 3–32	7.53	F	1	90	90							Subvertical, bifurcating, diffuse fault affecting sapropel
1H-6, 4–6	7.54	F	1.2	52	270							Normal in banded sapropel
1H-6, 4–12	7.54	F	1	58	270							Normal in banded sapropel
1H-6, 47–66	7.97	F	5	90	90							Subvertical, bifurcating, diffuse, irregular fault
8X-1, 2–6	140.02	V_1		52	270	0	24	54	294			Gypsum
8X-1, 5	140.05	V_2		0	90	0	0	Horizontal				Gypsum
8X-1, 9–10	140.09	SB_1		5	90	14	0	15	19			Gypsum
8X-1, 33–35	140.33	V_3		18	270	17	180	24	227			Gypsum
8X-1, 37–39	140.37	V_4		14	270	13	180	19	227			Gypsum
8X-1, 43–44	140.43	V5		10	270	27	180	28	199			Gypsum
8X-1, 44–50	140.44	V6		73	90	0	171	73	81			Gypsum
8X-1, 56–59	140.56	V7		30	90	0	159	32	69			Gypsum
8X-1, 72–73	141	SB_2		0	90	6	180	6	180			Blue breccia/conglomerate layer
9X-1, 2–4	145	V		51	90	42	180	57	126			Gypsum
9X-1, 5–7	144.95	V		18	270	8	180	19	247			Gypsum
9X-1, 8	144.98	V		2	270	6	180	6	198			Gypsum
9X-1, 9–10	144.99	V		11	270	7	180	13	238			Gypsum
9X-1, 18–19	145.08	SB		23	90	25	0	32	42			Gypsum gravel

Note: Feature symbols defined in Table 2 ("Explanatory Notes" chapter, this volume).

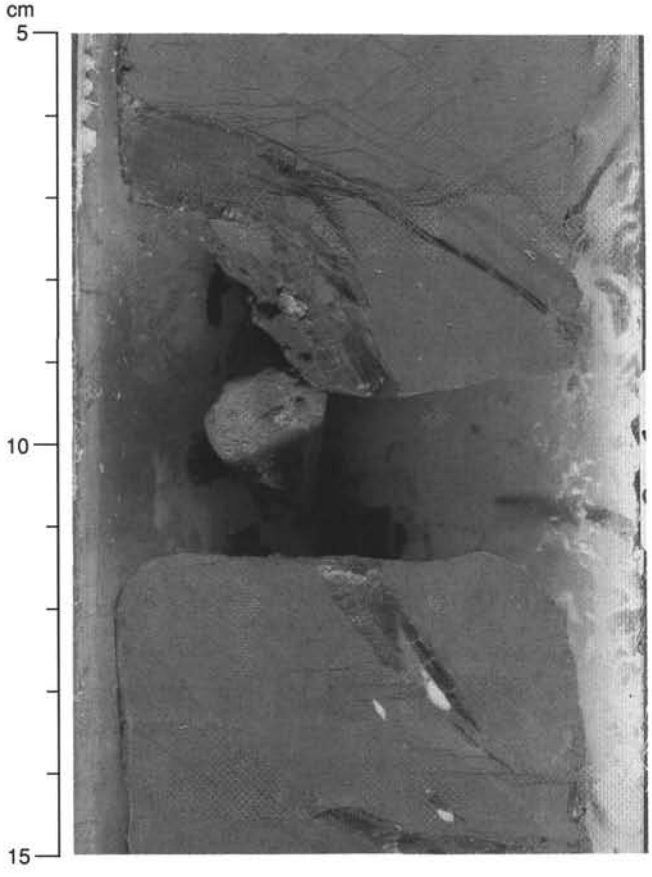

Figure 22. Example of tension gashes filled with gypsum from Section 160-973A-16X-1, 5–15 cm.

mm; see Fig. 16). In some of the larger microveins (up to 15 mm), which are only partially filled with fibrous gypsum, void space remains (Fig. 22).

The morphology of the gypsum varies considerably. Lenticular tension gashes, typically joined by sets of small-scale en echelon fractures (at about 30°–40° angles), are common in Core 160-973A-16X. Some of these are kinked to steeper angles with respect to the initial fissure (Fig. 22). Other morphologies include small (<1–5 mm) subrounded patches found in strands crosscutting the core and a thicker layer of gypsum that may have replaced an organic-rich layer in Core 160-973A-16X (see "Lithostratigraphy" section, this chapter). All the gypsum found in the cores is thought to be a secondary precipitate from sulfate-rich pore fluids (see "Inorganic Geochemistry" section, this chapter). However, the tension-gash morphology and crosscutting relationships of the veins indicate that these rocks have been affected by shear, possibly in more than one orientation.

Discrete beds of angular to subangular clasts were observed at the base of Hole 973D (e.g., Sections 160-973D-9X-1, 4–10 cm, 42–49 cm, 55–59 cm, and 72–73 cm). These beds both contain gypsum within the clasts and are cemented by it (Fig. 23). Crosscutting sets of submillimeter-sized gypsum microveins and tension gashes are present.

The systematic orientation of bedding to the southwest is consistent with the northwest-southeast strike of the Mediterranean Ridge in this region. The variation in orientation of the bedding planes may be the result of synsedimentary changes in slope associated with accretion processes.

Because of the poor recovery, only limited interpretation of the structural data can be made in the deeper part of Holes 973A and

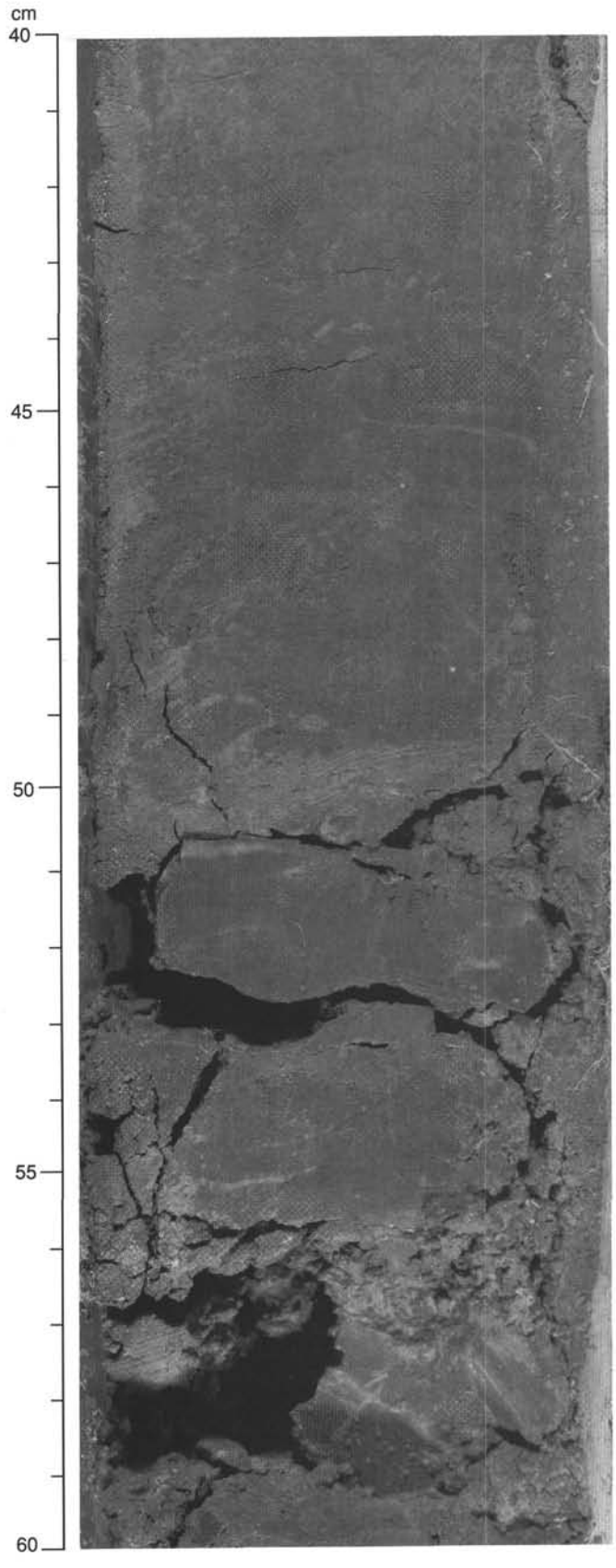

Figure 23. Thin brecciated intervals at Section 160-973D-9X-1, 40–60 cm.

973D. However, there is clear evidence for a marked increase in the intensity of deformation at the base of both these deeper holes. Evidence for large-scale shear was not preserved in the cores recovered, although horizontal to subhorizontal reflectors in the pre-site-survey seismic profiles (see Fig. 3, "Site Geophysics" section, this chapter) at 140–150 mbsf might suggest the occurrence of a fault zone around this depth. The reverse faulting found over this interval, though impossible to orient, is in good accordance with the tectonic environment of the toe of the Mediterranean Ridge accretionary complex.

COMPOSITE DEPTHS

High-resolution (2–10-cm scale) data collected on whole cores using the MST and percent color reflectance collected on split cores from Holes 973A, 973C, 973D, and 973E were used to determine depth offsets in the composite section. On the composite depth scale, sedimentary features present in adjacent holes were aligned so that they occur at approximately the same depth. Working from the top of the sedimentary sequence, a constant was added to the depth in meters below seafloor for each core in each hole to arrive at a composite depth for that core. The depth offsets that form the composite depth section are given in Table 5.

Percent color reflectance (collected at 2-cm intervals) and magnetic susceptibility data (collected at 3-cm intervals) were the primary parameters used for correlation purposes at this site. Natural gamma-ray data (collected at 10-cm intervals) and GRAPE wet-bulk density data (collected at 2-cm intervals) provided supplementary verification of core overlap and depth offsets. The percent color reflectance records (550-nm wavelength) and magnetic susceptibility data used to verify core overlap of the sedimentary section at Site 973 are shown on a composite depth scale in Figures 24 and 25, respectively. The continuity of the sedimentary sequence, in terms of core overlap, was documented for the interval from 0 to 55 mcd in Holes 973A, 973C (one core), 973D, and 973E (two cores). Interhole comparison of the MST data could not verify complete overlap between 55 and 65 mcd (Cores 160-973A-7H and 160-973D-7H) but could not discount it either, as no apparent gaps exist in the data. Composite section construction was not attempted below 65 mcd as core recovery was insufficient to provide hole-to-hole correlation.

Stretching and compression of the sedimentary features in aligned cores indicates distortion of the cored sequence resulting from coring disturbance and/or variations in the sedimentation rate between holes. As with other Leg 160 sites, much of the distortion occurs within individual cores on depth scales of less than 9 m, and it was not possible to align many features in the color reflection and magnetic susceptibility records accurately by simply adding a constant to the mbsf core depth. Within-core depth-scale changes will require post-cruise processing to align many of the sedimentary features.

Following construction of the composite depth section for Site 973, a spliced record was assembled from the aligned cores. The Site 973 spliced record can be used as sampling guide to recover a single sedimentary sequence. The spliced record consists of cores from Holes 973A, 973C, 973D, and 973E. Intervals with significant disturbance or distortion were avoided where possible. The tie points for the splice are given in Table 6. A small (20 cm) depth discrepancy may result when comparing composite depths generated from the offset depth table (Table 5) with composite depths of a single downcore record (e.g., percent color reflectance) generated using the splice table (Table 6). This discrepancy results from within-core misalignments of stratigraphic features used to make the splice (see discussion in previous paragraph).

Table 5. Site 973 composite depth section.

Core	Depth (mbsf)	Offset (m)	Depth (mcd)
160-973A-			
1H	0.00	0.60	0.60
2H	8.00	0.52	8.52
3H	17.50	1.39	18.89
4H	27.00	2.58	29.58
5H	36.50	3.82	40.32
6H	46.00	5.40	51.40
7H	55.50	5.40	60.90
160-973C-			
1H	0.00	1.10	1.10
160-973D-			
1H	0.00	0.00	0.00
2H	8.90	0.37	9.27
3H	14.90	2.68	17.58
4H	24.40	1.60	26.00
5H	33.90	2.28	36.18
6H	43.40	2.58	45.98
7H	52.90	2.58	55.48
160-973E-			
1H	13.00	0.36	13.36
2H	22.50	1.52	24.02

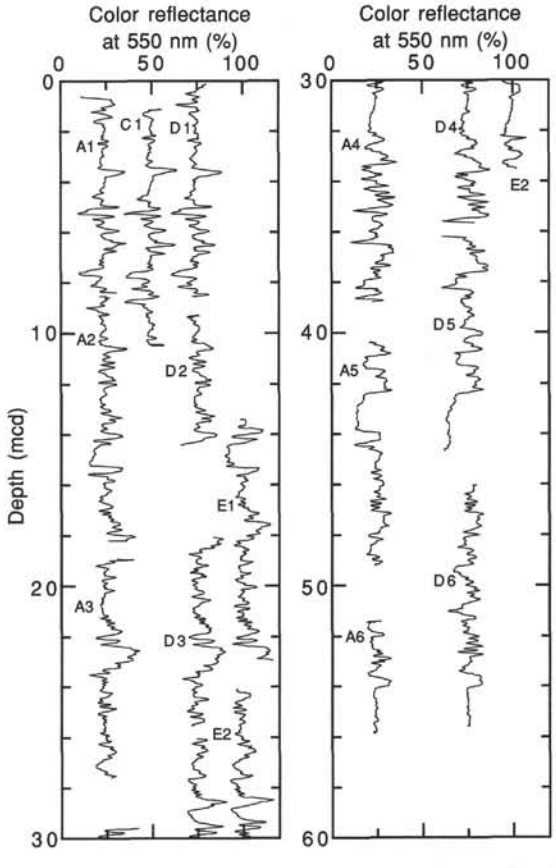

Figure 24. Percent color reflectance (550-nm wavelength) from Site 973 on the composite depth scale. The holes are offset from each other by a constant (25%). Cores for each hole are shown (e.g., D2 = Core 160-973D-2H).

INORGANIC GEOCHEMISTRY

Interstitial-water samples were obtained at Sites 972 and 973 from 5.90 to 142.83 mbsf, using the standard ODP titanium/stainless-steel squeezer (Manheim and Sayles, 1974) and a plastic-lined squeezer (Brumsack et al., 1992). In total, 24 samples were retrieved from both sites and subsequently analyzed for salinity, alkalinity, chloride, sulfate, lithium, potassium, calcium, magnesium, and bromide using the methods described in the "Explanatory Notes" chapter (this volume). Results of the analyses are in Table 7. Both sites are discussed in this section because their fluid regime and, therefore, pore-water chemistry are largely similar. Only the brine-related aspects of the pore-wa-

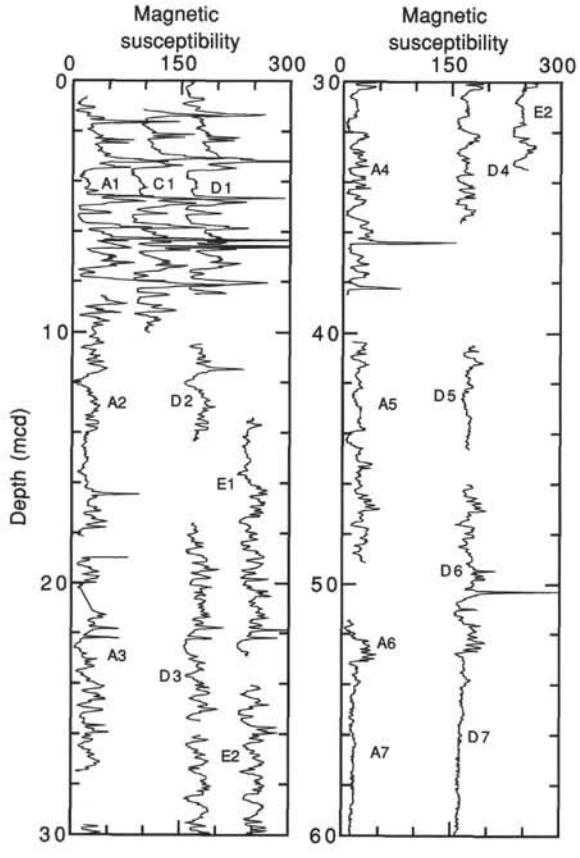

Figure 25. Magnetic susceptibility data (uncorrected instrument units) from Site 973 on the composite depth scale. The holes are offset from each other by a constant (75 instrument units). Cores for each hole are shown (e.g., D2 = Core 160-973D-2H).

ter chemistry will be discussed, because parameters relevant to organic matter degradation could not be analyzed owing to time constraints.

Salinity, Chloride, and Sodium

Both sites are characterized by steep increases in salinity with depth; a maximum value of 370 g/kg was recorded for the lowermost sample (142.83 mbsf) recovered at Site 973 (Fig. 26). The salinity increase is paralleled by high chloride concentrations of >5500 mM. In contrast to the other Leg 160 sites investigated during Leg 160, the sodium concentrations do not parallel the salinity variations with depth at Site 973 (Fig. 26). Instead, the magnesium concentrations increase to extremely high values (see below). The decrease in the sodium/chloride ratio from almost the seawater value of 0.86 in the uppermost samples to less than 0.1 downhole suggests that brine with a low sodium content is located at depth (Fig. 26).

Calcium, Sulfate, and Alkalinity

The calcium profile at both sites is characterized by steep concentration increases down to about 100 mbsf (Fig. 27), where gypsum veins occur (see "Lithostratigraphy" section, this chapter). A significant decrease in calcium is seen only in the lowermost samples of Site 973.

Sulfate concentrations are high at both sites. Low sulfate values were found between 100 and 130 mbsf, whereas an increase in sulfate in the lowermost intervals sampled at Site 973 must be related to upward diffusion from deeper downhole (Fig. 27). The decrease in calcium and the increase in sulfate and alkalinity are most likely the result of carbonate dissolution or dolomitization reactions at depth and gypsum precipitation in the interval below 100 mbsf (Fig. 27). The alkalinity buildup at depth may also be, in part, related to bacterial methane consumption, because methane concentrations increase slightly in the lower sections of Site 973 (see "Organic Geochemistry" section, this chapter).

Table 6. Site 973 splice tie points.

Hole, core, section, interval (cm)	Depth (mbsf)	Depth (mcd)		Hole, core, section, interval (cm)	Depth (mbsf)	Depth (mcd)
973D-1H-5, 70.0	6.70	6.70	ties to	973C-1H-4, 110.0	5.60	6.70
973C-1H-7, 8.0	9.08	10.18	ties to	973A-2H-2, 16.0	9.66	10.18
973A-2H-5, 84.0	14.84	15.36	ties to	973E-1H-2, 50.0	15.00	15.36
973E-1H-6, 94.0	21.44	21.80	ties to	973A-3H-3, 78.0	20.41	21.80
973A-3H-6, 76.0	24.89	26.28	ties to	973D-4H-1, 28.0	24.68	26.28
973D-4H-3, 136.0	28.76	30.36	ties to	973A-4H-1, 78.0	27.78	30.36
973A-4H-6, 128.0	35.78	38.36	ties to	973D-5H-2, 68.0	36.08	38.36
973D-5H-5, 50.0	40.16	42.44	ties to	973A-5H-2, 62.0	38.62	42.44
973A-5H-6, 92.0	43.32	47.14	ties to	973D-6H-1, 116.0	44.56	47.14
Append Core 160-973D-7H to Core 160-973D-6H						

Magnesium, Bromide, Potassium, and Lithium

In contrast to calcium, magnesium increases toward the bottom of both holes (Fig. 28). The concentrations are extremely high, reaching more than 40 times the seawater value in the lowermost sample from Site 973. This downhole increase implies that a magnesium-rich brine must be located at this depth, an assumption that is supported by the almost constant magnesium/chloride ratio of deeper samples from both sites (Fig. 28).

Bromide concentrations increase steeply with depth at the two sites (Fig. 28) and are higher than the sulfate concentrations in the deepest samples retrieved. The bromide/chloride ratio reflects this increase (Fig. 28). Both elements are indicative of late-stage evaporite brines.

The alkali metals potassium and lithium both increase with depth (Fig. 29), but display a slightly different behavior at the two sites. The potassium increase is much more pronounced at Site 973 than at Site 972, as seen in the potassium/chloride ratio (Fig. 29), which is almost constant at Site 973 and decreases to one-half the seawater value at Site 972. The lithium concentrations are similar in both holes down to 80 mbsf. The steep increase evident in the deeper levels of Site 973 may be related to a lithium-rich brine or processes of organic matter degradation and ammonium production. Unfortunately, ammonium could not be determined owing to time constraints.

In conclusion, it is clear that the pore-water chemistry at Sites 972 and 973 is dominated by upward diffusion or even advection of a late-stage evaporite brine. This magnesium-, sulfate-, and bromide-rich brine dominates diagenetic reactions occurring in the sedimentary column, in particular at the depth interval where gypsum precipitation is presently taking place.

ORGANIC GEOCHEMISTRY

Volatile Hydrocarbons

As part of the shipboard safety and pollution-prevention monitoring program, hydrocarbon gases were analyzed in Hole 973A by the headspace technique. Only minor concentrations of methane in the range of 3 to 86 ppm were recorded. The results are reported in Table 8. Methane concentrations were very low down to about 100 mbsf. Below this depth, slightly higher methane concentrations were found.

Carbon, Nitrogen, and Sulfur

The abundances of total, inorganic, and organic carbon, calcium carbonate, and total nitrogen and sulfur in sediments from Hole 973A

Table 7. Results of pore-water analysis for Sites 972 and 973.

Core, section, interval (cm)	Depth (mbsf)	pH	Alkalinity (meq/L)	Salinity (g/kg)	Cl^- (mM)	Mg^{2+} (mM)	Ca^{2+} (mM)	SO_4^{2-} (mM)	K^+ (mM)	Br^- (mM)	Li^+ (μM)	Na^+ (mM)
160-972A-												
1H-4, 145–150	5.95	7.50	3.669	43.7	687	82.6	18.9	32.3	11.7	1.5	32	479
2H-4, 145–150	15.45	7.27	2.807	56.3	894	154.0	37.3	32.5	12.9	2.6	45	499
3H-4, 110–120	24.60	7.12	2.316	74.3	1135	248.0	62.3	38.6	14.8	4.4	53	511
4H-4, 140–150	34.40	6.46	1.825	93.8	1438	366.0	97.7	39.0	17.2	6.5	66	601
5H-4, 140–150	43.90	6.57	1.553	112.0	1734	491.0	131.0	28.7	19.3	8.8	71	676
6H-4, 140–150	53.40	6.54	2.247	128.3	1983	559.0	154.0	31.3	21.9	10.3	73	663
7H-4, 140–150	62.90	6.54	1.131	143.8	2257	668.0	187.0	26.0	24.7	11.6	76	707
8X-4, 140–150	72.40	6.51	1.424	159.0	2480	723.0	208.0	23.7	27.0	13.6	78	696
9X-1, 135–150	77.45	6.49	1.225	163.0	2693	785.0	230.0	26.0	29.8	16.8	81	748
10X-3, 135–150	90.05	6.27	0.860	190.0	3032	848.0	255.0	17.2	33.4	19.1	78	678
160-973A-												
1H-4, 140–150	5.90	7.39	2.928	44.0	691	93.0	20.4	36.70	13.7	1.4	41.0	511
2H-4, 140–150	13.90	7.29	2.637	52.5	824	146.0	33.8	38.20	16.0	2.6	43.0	506
3H-1, 140–150	18.90	7.15	2.400	60.5	925	192.0	45.9	34.60	18.7	2.2	46.1	503
4H-4, 140–150	32.90	6.81	2.071	82.0	1228	315.0	76.1	35.10	25.3	5.7	53.9	491
5H-2, 140–150	39.40	6.68	1.922	94.0	1438	378.0	92.6	39.90	30.3	8.0	58.5	481
6H-4, 140–150	51.90	6.42	1.789	115.0	1765	533.0	129.0	34.40	35.8	9.9	64.2	478
7H-4, 140–150	61.40	6.74	2.826	131.5	1993	630.0	153.0	32.10	40.5	11.0	70.4	483
8X-2, 140–150	67.90	6.44	2.066	141.8	2194	770.0	189.0	31.80	43.5	13.2	73.5	466
9X-1, 0–10	74.50	6.66	2.835	155.8	2438	807.0	197.0	29.60	46.4	14.7	77.7	476
12X-CC, 0–1	103.30	—	—	208.0	3448	1298.0	218.0	20.6	69.93	25.2	110.8	476
13X-2, 135–150	115.75	5.97	6.663	257.0	4016	1641.0	177.0	19.8	82.50	31.2	132.0	476
14X-4, 130–150	128.30	6.09	8.541	273.0	4228	1770.0	130.0	26.0	86.64	34.8	142.3	443
15X-1, 0–10	132.10	6.11	9.734	283.0	4396	1715.0	101.0	32.0	93.08	41.3	154.2	433
16X-1, 113–123	142.83	5.76	17.389	370.0	5504	2228.0	15.0	37.8	112.86	52.2	365.0	433

Note: — = no data.

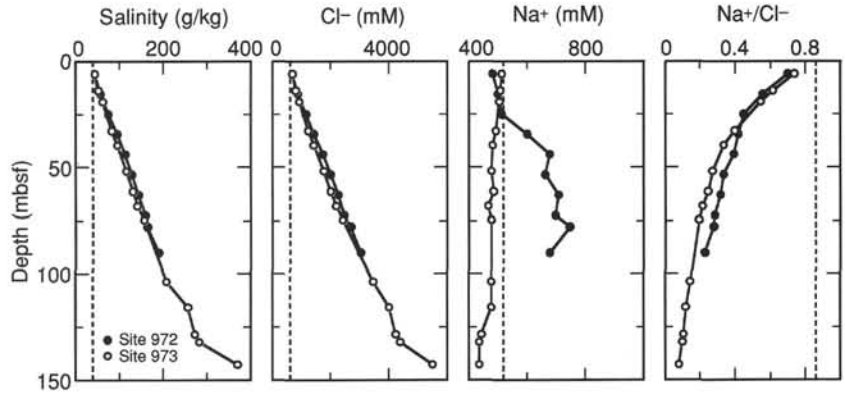

Figure 26. Pore-water vs. depth profiles at Sites 972 and 973 for salinity, chloride, sodium, and sodium/chloride ratio. The dashed line indicates the bottom-water concentration.

are summarized in Table 9. Random sampling was performed for Hole 973A, with additional samples taken from the dark sapropels.

The carbonate contents measured are highly variable and range from 3% in a black sapropel to 74% in background nannofossil ooze (Fig. 30). Carbonate content is very low in those sapropels richest in organic matter (>10% C_{org}) in Sections 160-973A-1H-4, 4H-3, 4H-5, and 8X-1, but otherwise is mostly in the range of the adjacent background sediment.

Organic carbon values in Hole 973A are highly variable in the sapropels (Table 9, Fig. 30). The maximum value of 18.5% was measured in Sample 160-973A-8X-1, 120–121 cm. The composition of the organic matter in the sandstone with black laminae and clasts (Section 160-973A-9X-1) is different from that of the sapropels with respect to nitrogen and sulfur contents. The black material most likely represents redeposited sapropel that was oxidized during erosion and transport, thereby losing the most labile (sulfur and nitrogen) components. Shore-based analysis should also determine if the material is solid bitumen.

C_{org}/N ratios in sapropels vary from 13.2 to 20.6 (disregarding the sandstone sample from Section 160-973A-9X-1; Table 9). As observed at other sites (see, e.g., "Organic Geochemistry" section, "Site 964," "Site 966," and "Site 967" chapters, this volume), the surpris-

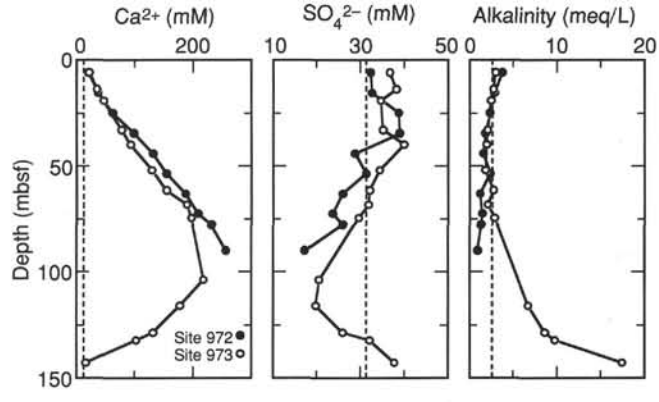

Figure 27. Pore-water vs. depth profiles at Sites 972 and 973 for calcium, sulfate, and alkalinity. The dashed line indicates the bottom-water concentration.

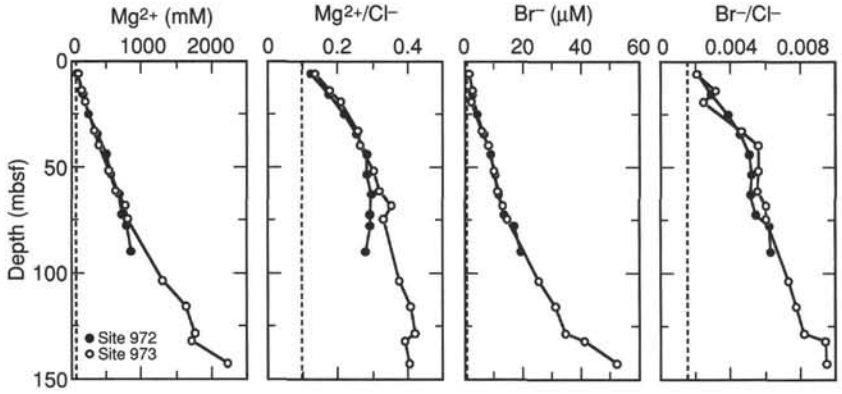

Figure 28. Pore-water vs. depth profiles at Sites 972 and 973 for magnesium, magnesium/chloride ratio, bromide, and bromide/chloride ratio. The dashed line indicates the bottom-water concentration.

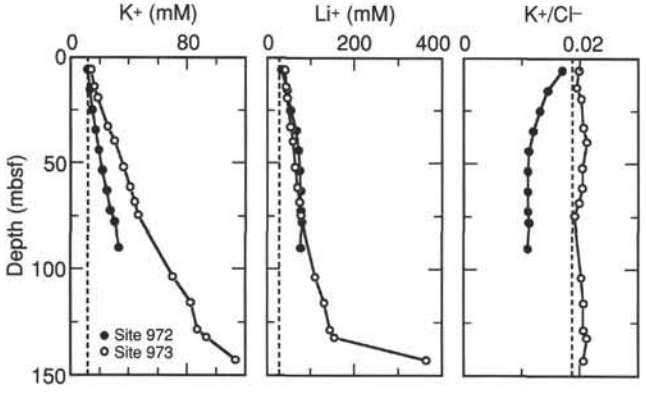

Figure 29. Pore-water vs. depth profiles at Sites 972 and 973 for potassium, lithium, and potassium/chloride ratio. The dashed line indicates the bottom-water concentration.

Table 8. Hydrocarbon gas data for Hole 973A, headspace method.

Core, section, interval (cm)	Depth (mbsf)	C_1 (ppm)
160-973A-		
1H-5, 0–5	6.00	4
2H-5, 0–5	14.00	3
3H-2, 0–5	19.00	4
4H-5, 0–5	33.00	3
5H-3, 0–5	39.50	4
6H-5, 0–5	52.00	5
7H-5, 0–5	61.50	8
8X-3, 0–5	68.00	7
9X-1, 0–5	74.50	4
13X-2, 0–5	114.40	51
14X-5, 0–5	128.50	86
15X-1, 11–16	132.21	15
16X-1, 0–5	141.70	34

ingly high values of the C_{org}/N ratio in many of the sapropels suggest a predominance of terrestrial organic matter. The high C_{org}/N ratios in the sapropels are again tentatively interpreted as representing an effective removal of nitrogen compounds from the marine organic matter during diagenesis. However, the possibility that the primary marine organic matter was already poor in nitrogen-bearing constituents at the time of deposition cannot be excluded.

Sulfur values are reported in Table 9. Sulfur concentrations vary from about 2% to 30% in the sapropels, but are not closely related to organic carbon content. An exception is the organic matter in the sandstone in Section 160-973A-9X-1, which is sulfur poor.

PHYSICAL PROPERTIES

A nearly complete suite of physical and index properties (see "Explanatory Notes" chapter, this volume) was measured in all cores from Hole 973A. Thermal conductivity measurements were canceled to allow early splitting and description of the cores. The MST was run on all cores from Hole 973D. In this section, we describe the downhole distribution of physical properties of Hole 973A.

Index Properties

Bulk and dry density were measured on every section of the unconsolidated sediment down to 60 mbsf. Density generally increases with depth, with a sharp increase of the dry and bulk density at the 0–4 mbsf interval followed by a moderate increase (Table 10, Fig. 31). Water content and porosity display a mirror image of the index properties density values. Water content decreases from about 45% at the seafloor to 26% at approximately 60 mbsf, and the porosity decreases from about 68% to 47% at the same depths (Table 10, Fig. 31).

Discrete-sample *P*-wave and Shear Strength Measurements

Horizontal and vertical *P*-wave velocities, measured with the digital sonic velocimeter, show a generally increasing trend with depth in Hole 973A (Table 11, Fig. 32), from 1.5 km/s at the seafloor to 1.7 km/s at 57 mbsf. The change in lithology from unconsolidated to partly consolidated sediments is associated with a few DSV 3 velocity measurements that range from 1.75 km/s at 66 mbsf to 2.45 km/s at 132 mbsf. Vane shear strength shows a similar pattern with depth, ranging between 1 and 105 kPa for a depth range of 0–57 mbsf (Table 12, Fig. 32).

GRAPE Density

The overall trend of the GRAPE data (Fig. 33) is toward slightly increasing density to a depth of 60 mbsf. The ooze and sapropel complex down to 47 mbsf shows wider fluctuations than the turbidites underneath at 57–65 mbsf (see "Lithostratigraphy" section, this chapter). The lower density values measured in the partly consolidated clays from below 65 mbsf probably result from liners that were only partially filled. A comparison of the index properties density measurements (Fig. 33) with GRAPE density suggests that the GRAPE measurements in this hole underestimate density, despite application of the Boyce correction (see "Explanatory Notes" chapters, this volume, and as discussed in the "Physical Properties" section, "Site 967" chapter, this volume). The large discrepancy below 65 mbsf is related to XCB coring and core liners that are not completely filled with material.

Table 9. Concentration of total, inorganic, and organic carbon, calcium carbonate, total nitrogen, and sulfur in sediments from Hole 973A.

Core, section, interval (cm)	Depth (mbsf)	Total carbon (%)	Inorganic carbon (%)	Organic carbon (%)	$CaCO_3$ (%)	Nitrogen (%)	Sulfur (%)	C_{org}/N	C_{org}/S
160-973A-									
1H-1, 66–67	0.66		4.38		36.49				
1H-4, 11–12	4.61	14.39	0.98	13.41	8.16	0.84	8.08	15.9	1.7
1H-4, 22–23	4.72		8.10		67.47				
1H-5, 98–99	6.98	8.07	4.70	3.37	39.15	0.22	3.68	15.2	0.9
1H-5, 113–114	7.13		3.71		30.90				
1H-6, 2–3	7.52	9.22	4.49	4.73	37.40	0.30	4.19	15.6	1.1
2H-1, 47–48	8.47	6.78	4.46	2.32	37.15	0.17	2.81	13.7	0.8
2H-1, 60–61	8.60		3.90		32.49				
2H-3, 60–61	11.60		4.88		40.65				
2H-4, 38–39	12.88		3.71		30.90				
2H-4, 41–42	12.91		7.67		63.89				
2H-5, 106–107	15.06	5.94	3.84	2.10	31.99	0.16	4.73	13.2	0.4
2H-6, 60–61	16.10		2.74		22.82				
3H-1, 60–61	18.10		4.54		37.82				
3H-4, 60–61	21.73	8.40	7.80	0.60	64.97	0.20	2.68		
3H-4, 98–99	22.11		5.42		45.15				
3H-4, 103–104	22.16		3.61		30.07				
3H-6, 57–58	24.70		4.53		37.73				
4H-1, 78–79	27.78		6.50		54.15				
4H-3, 83–84	30.83	18.06	0.79	17.27	6.58	0.84	6.70	20.6	2.6
4H-4, 20–21	31.70	11.02	5.48	5.54	45.65	0.33	2.86	16.8	1.9
4H-4, 111–112	32.61	10.37	6.29	4.08	52.40	0.24	2.93	16.8	1.4
4H-5, 40–41	33.40		3.80		31.65				
4H-5, 86–87	33.86	17.94	0.71	17.23	5.91	0.91	8.43	19.0	2.0
4H-6, 119–120	35.69	12.61	6.76	5.85	56.31	0.30	2.05	19.8	2.9
5H-1, 60–61	37.10	11.33	3.60	7.73	29.99	0.48	4.02	16.3	1.9
5H-2, 45–46	38.45		8.08		67.31				
5H-3, 58–59	40.08	10.43	5.74	4.69	47.81	0.28	2.39	16.6	2.0
5H-6, 45–46	42.85		3.75		31.24				
5H-6, 58–59	42.98		7.14		59.48				
6H-2, 18–19	47.68		0.97		8.08				
6H-2, 100–101	48.50		7.12		59.31				
7H-1, 40–41	55.90		6.71		55.89				
7H-5, 40–41	61.90		7.51		62.56				
8X-1, 26–27	65.26	9.67	0.38	9.29	3.17	0.53	4.09	17.7	2.3
8X-1, 72–73	65.72	8.00	0.93	7.07	7.75	0.47	5.25	15.1	1.3
8X-1, 120–121	66.20	18.79	0.26	18.53	2.17	0.94	30.37	19.7	0.6
8X-3, 56–57	68.56		7.08		58.98				
8X-4, 40–41	69.90		7.38		61.48				
9X-1, 82–83	75.32	10.93	6.84	4.09	56.98	0.15	0.34	27.4	12.2
13X-1, 76–77	113.66		7.22		60.10				
13X-CC, 21–22	116.11		8.07		67.20				
14X-2, 50–51	124.50		8.91		74.20				
14X-5, 50–51	129.00		5.33		44.40				
15X-1, 29–30	132.39		7.94		66.10				
16X-1, 30–39	142.00		1.28		10.66				

Compressional Wave Velocities

High-resolution compressional wave velocities were measured using the PWL of the MST (Fig. 34). The velocity increases with depth from 1.5 to 1.75 km/s at a constant rate over the measured interval to 65 mbsf. Comparison with the DSV measurements shows good agreement.

Magnetic Susceptibility

Figure 35 shows the results of magnetic susceptibility measurements from Hole 973A. The values decrease in the ooze and sapropel complex down to 47 mbsf, showing a wide range of data dispersion. In the turbidites at 47–65 mbsf susceptibility values continue their decrease, but at a reduced amount of dispersion. In the lower part of Hole 973A, susceptibility varies at about 10^{-4} SI units.

Natural Gamma-ray Radiation

NGR values, measured using the MST, from Hole 973A show a moderate decrease from 30 to 24 counts per second (cps) from the seafloor to 65 mbsf, but the ooze and sapropel complex (0–47 mbsf) is distinguished by a larger range of variation than the turbidites at 47–65 mbsf (Fig. 36). In the lower part of Hole 973A, NGR values are relatively low.

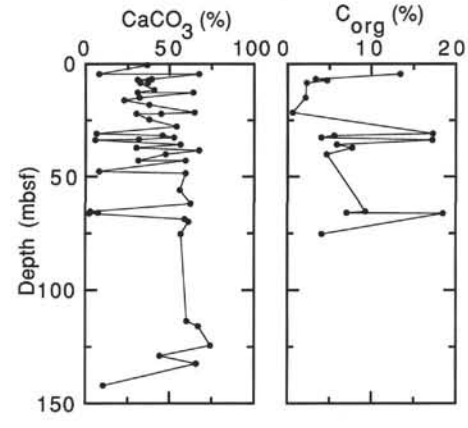

Figure 30. Downhole distribution of calcium carbonate and organic carbon concentrations for samples from Hole 973A.

Correlation with Lithostratigraphy

The two lithostratigraphic units of Hole 973A (see "Lithostratigraphy" section, this chapter)—the ooze and sapropel complex down to 47 mbsf and the turbidites at 57–65 mbsf—can be clearly distin-

Table 10. Index properties measured in cores from Hole 973A.

Core, section, interval (cm)	Depth (mbsf)	Water content (wt%)	Porosity (vol%)	Bulk density (g/cm^3)		Grain density (g/cm^3)		Dry density (g/cm^3)	
				Method B	Method C	Method B	Method C	Method B	Method C
160-973A-									
1H-1, 50–52	0.50	44.73	68.52	1.61	1.57	3.00	2.76	0.89	0.87
1H-3, 50–52	3.50	32.25	55.91	1.81	1.78	2.87	2.73	1.23	1.20
1H-5, 50–52	6.50	37.04	60.66	1.72	1.68	2.85	2.69	1.08	1.06
2H-1, 105–107	9.05	38.71	63.10	1.67	1.67	2.79	2.77	1.03	1.02
2H-3, 89–91	11.89	35.63	59.79	1.78	1.72	2.99	2.75	1.14	1.11
2H-5, 59–61	14.59	23.80	44.70	2.03	1.92	2.92	2.65	1.54	1.47
3H-1, 85–87	18.35	34.55	59.03	1.80	1.75	2.98	2.80	1.18	1.15
3H-3, 70–72	20.33	35.02	58.47	1.77	1.71	2.90	2.68	1.15	1.11
3H-5, 104–106	23.67	33.98	57.21	1.75	1.72	2.77	2.66	1.16	1.14
4H-1, 72–74	27.72	31.03	54.32	1.84	1.79	2.87	2.71	1.27	1.24

Only part of this table is reproduced here. The entire table appears on the CD-ROM (back pocket).

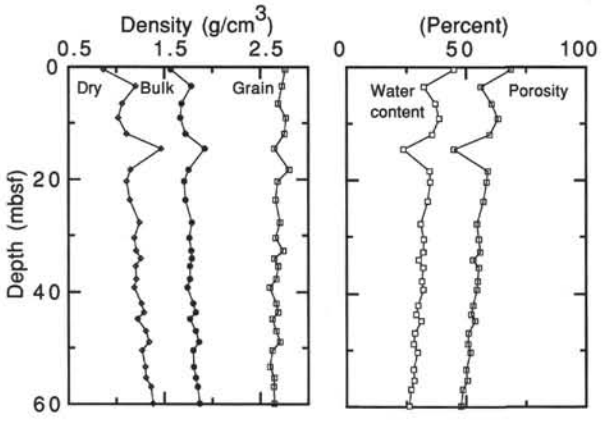

Figure 31. Index properties measured in cores from Hole 973A. Density was calculated using method C (see "Explanatory Notes" chapter, this volume).

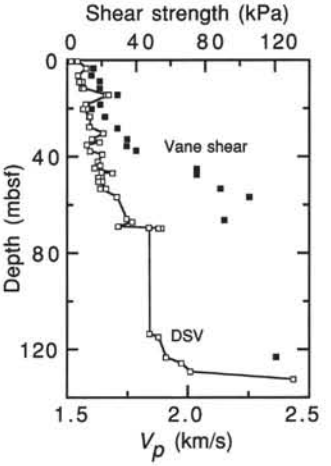

Figure 32. *P*-wave velocity (using DSV 1, 2, and 3) and vane shear strength measured in cores from Hole 973A.

Table 11. Compressional wave velocity measured in split cores from Hole 973A.

Core, section, interval (cm)	Depth (mbsf)	Measurement type	Velocity (km/s)
160-973A-			
1H-1, 52.2	0.52	DSV 2	1.54
1H-1, 53.5	0.53	DSV 1	1.52
1H-3, 49.9	3.50	DSV 1	1.58
1H-3, 55.2	3.55	DSV 2	0.79
1H-5, 49.6	6.50	DSV 1	1.55
2H-1, 98.9	8.99	DSV 1	1.56
2H-1, 99.7	9.00	DSV 2	1.55
2H-3, 81.7	11.82	DSV 1	1.56
2H-3, 82.5	11.82	DSV 2	1.57
2H-5, 49.4	14.49	DSV 1	1.66

Note: Direct DSV measurements.

Only part of this table is reproduced here. The entire table appears on the CD-ROM (back pocket).

Table 12. Vane shear strength measured in split cores from Hole 973A.

Core, section, interval (cm)	Depth (mbsf)	Strength (kPa)
160-973A-		
1H-1, 52.9	0.53	1.20
1H-3, 48.1	3.48	15.20
1H-5, 48.3	6.48	14.20
2H-1, 90.1	8.90	19.10
2H-3, 88.7	11.89	18.80
2H-5, 41.5	14.42	29.30
3H-1, 87.7	18.38	19.30
3H-3, 64.5	20.28	14.20
3H-5, 94.1	23.57	21.80
4H-1, 123.2	28.23	29.30

Only part of this table is reproduced here. The entire table appears on the CD-ROM (back pocket).

guished by their physical properties. The turbidites generally show lower variation in the data. Below 65 mbsf, the available information is not sufficient to allow interpretation.

DOWNHOLE MEASUREMENTS

Logging Operations and Quality of Logs

As a result of time constraints at Site 973, we acquired a reduced suite of log data by using the seismic-stratigraphic tool string of the Quad combination. We decided to run the Quad combo in two parts because of uncertainties about hole conditions. After running the seismic-stratigraphic string without encountering difficulties, there was not enough time left to run the litho-porosity string.

After coring and drilling operations were completed in Hole 973D, the borehole was conditioned with KCl drilling mud. The base of the BHA was set at 71.15 mbsf and pulled up to 52 mbsf. We logged between and 152 and 52 mbsf. Table 13 summarizes the information of the single logging run.

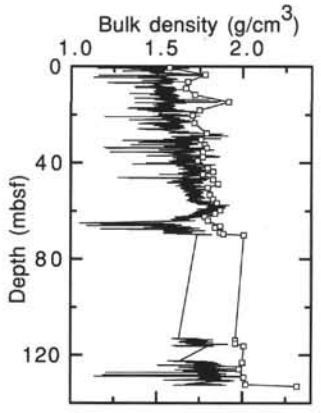

Figure 33. Density measured in Hole 973A as part of the index properties measurements (connected open symbols) and GRAPE density measured using the MST.

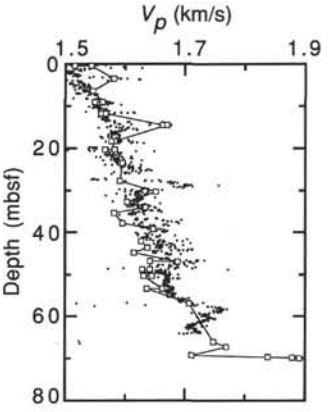

Figure 35. Magnetic susceptibility measured in cores from Hole 973A using the MST.

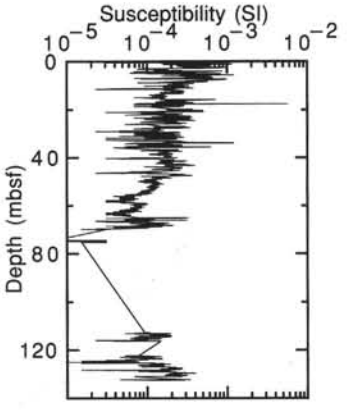

Figure 34. Compressional wave velocities measured in cores from Hole 973A using the PWL component of the MST (solid symbols) and the DSV (connected open symbols).

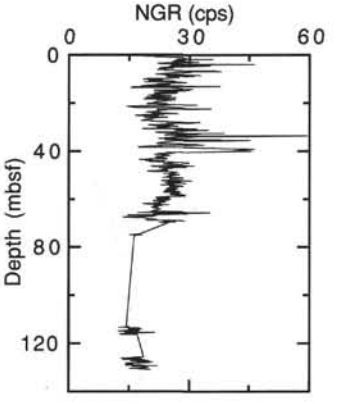

Figure 36. Natural gamma-ray radiation measured in cores from Hole 973A using the MST.

The logs appear to be of good quality (Fig. 37), although they can be used only on a qualitative basis as we did not record the borehole diameter, and borehole effects on the log values are unknown. The sonic log is generally of good quality, but needs reprocessing between 102 and 106 mbsf and between 128 and 135 mbsf. These intervals may correspond to major washout zones.

Results and Interpretation

Four main log intervals are identified on the basis of the log response: 52–83, 83–112, 112–128, and 128–152 mbsf. The boundaries that can be traced at 83, 112, and 128 mbsf represent interval boundaries where the sediments display different features and, thus, reflect significant changes within the sedimentary evolution in Hole 973D.

A remarkable feature is that the resistivity and sonic logs (the only porosity-sensitive logs available) indicate a clear compaction trend with depth.

The only logs available from the lowermost part of Hole 973D are those recorded by the dual induction tool, which indicate the presence of a relatively higher resistivity interval between 143 and 148 mbsf. The log response can be interpreted as a well-cemented level. The gypsum-rich and well-cemented materials recovered most likely give rise to this log response. To determine the lithology on the basis of the log values, additional lithology indicators (density, PEF) are necessary.

Between 52 and 83 mbsf, the gamma-ray logs display moderate radioactivity (20–55 GAPI). Intervals with a sharp change in radioactivity at the base and gradual increase or decrease in radioactivity upward can be interpreted in terms of normal and reverse graded sequences, respectively. These trends are also recognized (with less definition owing to the resolution of the dual induction tool) on the resistivity logs, which supports the interpretation suggested above.

Between 83 and 112 mbsf, an interval of almost no recovery, the log response indicates the existence of interbedded layers displaying abrupt changes in radioactivity and thus different composition. The high uranium values of the more radioactive intervals are comparable to those recognized and described for sapropel-rich intervals at other sites of this leg (e.g., see "Downhole Measurements" section, "Site 968" chapter, this volume). Both the sonic and the resistivity logs also show slightly higher values for these levels suggesting a different composition. The low-radioactivity layers might correspond either to relatively coarser grained material (silty or sandy) or to carbonate-rich sediments.

The interval between 110 and 128 mbsf displays relatively lower radioactivity (20–40 GAPI), higher resistivity, and acoustic velocity, which suggests a change in composition and probably also greater compaction and lower porosity.

Between 128 and 152 mbsf, an increase in resistivity and acoustic velocity indicates a significant compositional change in relation to

Table 13. Hole 973 logged depth intervals for the seismic-stratigraphic tool string.

String	Run	Open-hole depth (mbsf)	Open-hole depth (mbrf)	In-pipe depth (mbsf)	In-pipe depth (mbrf)	Tools
Seismic-stratigraphic	Up	153.5–52.6	3859.1–3758.2	52.6–0	3758.2–3705.6	NGT/SDT/DIT

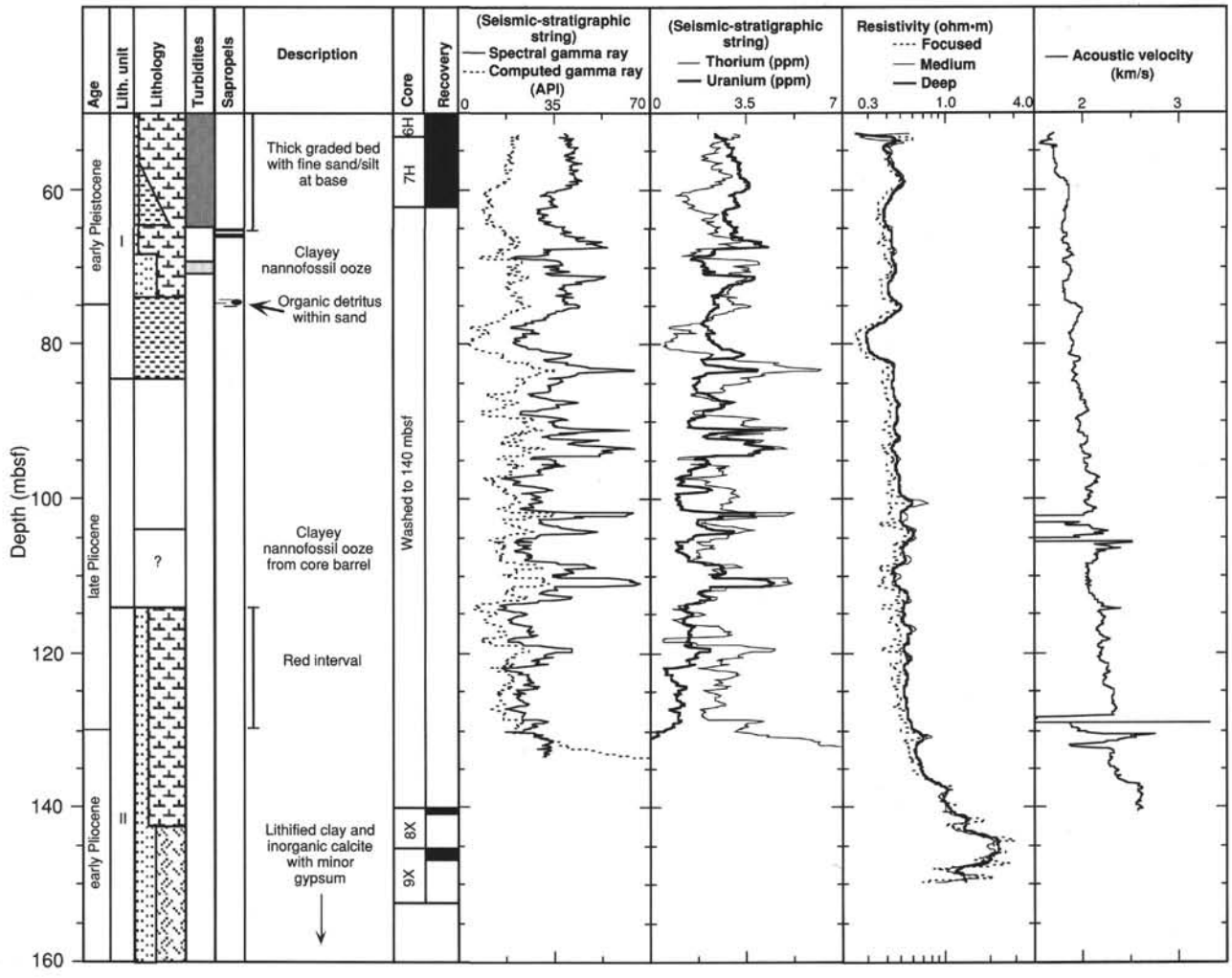

Figure 37. Seismic-stratigraphic Quad combination tool logs for Hole 973D.

the overlying sediments. The characterization of these materials on the basis of the log response is poor because this interval was logged only partially by the sonic and gamma-ray logging tools.

SUMMARY AND CONCLUSIONS

The objective of drilling at Site 973 was to investigate the structure, sedimentation, and geochemical environment of the lower toe of the Mediterranean Ridge accretionary prism. The site is located on a broad high slightly higher on the slope relative to Site 972. Two lithostratigraphic units were recognized as follows:

Unit I comprises 84 m of nannofossil ooze and nannofossil clay of late Pliocene to Holocene age with more than 27 intercalated sapropels. There are also interbeds of sands, silts, and nannofossil clays and a single 14-m-thick interval of sand that grades upward into nannofossil clay. The provenance of the sand was mainly foraminiferal lime mudstones. The turbidite-rich interval is distinguished on the downhole gamma-ray logs by progressive changes in log values (e.g., radioactivity). Three thin ash layers are present in the upper part of the section. Pleistocene planktonic foraminifers are generally common to abundant, whereas Pliocene forms are less diverse and moderately to poorly preserved. Reworking is common throughout.

Unit II is made up of approximately 68 m of red-colored clayey nannofossil ooze and an underlying calcareous silty claystone with a thin black layer almost completely replaced by gypsum that is interpreted as a relict sapropel. The unit is paleontologically dated as early to late Pliocene. Planktonic foraminifers are rare or absent. Downhole logs of this poorly recovered interval suggest the presence of alternations of relatively coarse- and fine-grained sediments. High uranium levels may indicate the presence of organic-rich layers (e.g., sapropels) above 112 mbsf.

The upper part of the section cored by APC was correlated among the holes based on the nature and occurrence of sapropels, turbidites, and distinctive ash layers. High-resolution reflectance data were used to check the visual correlations. Incomplete stratigraphic records

were attributed to coring gaps and the erosion and removal of some sapropels, possibly by the turbidity currents responsible for sand deposition.

Bedding in the upper part of the section recovered by APC generally dips shallowly to the south or southwest. Some steeply inclined normal faults occur locally with small offsets. Elsewhere, subvertical faults with offsets of up to 44 cm length were noted. Between 140 and 152.6 mbsf, microveins and small-scale reverse faults are infilled with fibrous gypsum. Several generations of crosscutting gypsum veins can be observed. The gypsum was also deformed by tension gashes linked with small-scale en echelon fractures. In addition, discrete beds of angular to subangular clasts were noted near the base of the recovered section.

The paleomagnetic data are dominated by normal polarity. However, paleontological studies indicate that about one-half of the cored intervals should exhibit reverse polarity. It may be possible to extract a useful magnetic polarity stratigraphy after detailed post-cruise studies.

Pore-water analyses record a sharp increase in salinity with depth, to a maximum level of 370 g/kg at the base of the recovered interval. Chloride parallels this increase, together with magnesium, but sodium decreases, suggesting that a brine with low sodium content may be present at depth. Calcium increases steeply down to the level where gypsum is present, and then decreases. Trends in sulfate, calcium, and alkalinity are interpreted in terms of the upward diffusion of sulfate, carbonate dissolution, or dolomitization reactions at depth and gypsum precipitation below 100 mbsf. Methane concentrations increase slightly downhole, and an alkalinity buildup at depth may in part be related to bacterial methane consumption. High levels of magnesium near the base of the recovered section (>40 times seawater concentration) imply that a magnesium-rich brine is located at this depth. Bromide concentrations also increase steeply with depth, suggesting the existence of a late-stage evaporite brine. All the gypsum present in Unit II is interpreted as a secondary precipitate from sulfate-rich pore waters, based on the textural evidence in the cores.

The sedimentation recorded at Site 973 began with the accumulation of nannofossil clays with sapropels in the early Pliocene. Red-colored clayey nannofossil ooze followed. Poor recovery in the upper Pliocene may have resulted from the presence of unlithified sands. Nannofossil oozes continued to accumulate in the Pleistocene with the periodic development of sapropels and deposition of silt and sand from turbidity currents, some of which were erosive. The provenance of the sand was largely from foraminiferal lime mudstones. Sapropels were not deposited during the middle-late Pleistocene when the reddish brown oxidized sediments accumulated. Sedimentation rates were calculated based solely on calcareous nannofossil events and range from 23 to 111 m/m.y, with six significant changes throughout the section.

The veins and tension gashes indicate that these rocks have been affected by shear, possibly in more than one orientation. The structural features and changes in bedding dips within the section indicate a downward increase in deformation toward a décollement beneath the toe of the Mediterranean Ridge accretionary complex.

REFERENCES

Brumsack, H.-J., Zuleger, E., Gohn, E., and Murray, R.W., 1992. Stable and radiogenic isotopes in pore waters from Leg 127, Japan Sea. *In* Pisciotto, K.A., Ingle, J.C., Jr., von Breymann, M.T., Barron, J., et al., *Proc. ODP, Sci. Results,* 127/128 (Pt. 1): College Station, TX (Ocean Drilling Program), 635–650.

Hirschleber, H.B., Hartmann, J.M., and Hieke, W., 1994. The Mediterranean Ridge accretionary complex and its forelands—seismic reflection studies in the Ionian Sea. *Cruise Report of the Meteor,* 120:491–509.

Manheim, F.T., and Sayles, F.L., 1974. Composition and origin of interstitial waters of marine sediments based on deep sea drill cores. *In* Goldberg, E.D. (Ed.), *The Sea* (Vol. 5): New York (Wiley Interscience), 527–568.

McCoy, F.W., Jr., 1974. Late Quaternary sedimentation in the Eastern Mediterranean Sea [Ph.D. thesis]. Harvard Univ., Cambridge, MA.

Sprovieri, R., 1993. Pliocene–early Pleistocene astronomically forced planktonic Foraminifera abundance fluctuations and chronology of Mediterranean calcareous plankton bio-events. *Riv. Ital. Paleontol. Stratigr.,* 99:371–414.

Ms 160IR-114

NOTE: Core-description forms ("barrel sheets") and core photographs can be found in Section 5, beginning on page 535. Forms containing smear-slide data can be found in Section 6, beginning on page 951. Color reflectance, physical properties, chemistry, and thin-section data are presented on the CD-ROM (back pocket).

SHORE-BASED LOG PROCESSING
HOLE 973D

Bottom felt: 3705.6 mbrf
Total penetration: 152.6 mbsf
Total core recovered: 64.1 m (85 %)

Logging Runs

Logging string 1: DIT/SDT-LSS/NGT
The wireline heave compensator was used to counter ship heave resulting from the mild sea conditions.

Bottom-hole Assembly

The following depth for the BHA is as it appears on the logs after differential depth shift (see **Depth shift** section) and depth shift to the seafloor. As such, there might be a discrepancy with the original depths given by the drillers onboard. Possible reasons for depth discrepancies are ship heave, use of wireline heave compensator, and drill string and/or wireline stretch.
DIT/SDT-LSS/NGT: bottom hole assembly @ 52.5 mbsf.

Processing

Depth shift: No differential depth shift was required. All original logs were depth shifted to the seafloor (3705.6 mbrf).

Gamma-ray processing: The NGT data were processed to correct for borehole size and type of drilling fluid.
Acoustic data processing: The sonic logs were processed to eliminate some of the noise and cycle skipping experienced during recording.

Quality Control

Data recorded through the BHA, such as the NGT data above 52.5 mbsf, should be used only qualitatively because of the attenuation on the incoming signal.
No hole diameter measurement was performed.
Details of standard shore-based processing procedures are found in the "Explanatory Notes" chapter (this volume). For further information about the logs, please contact:

Cristina Broglia
Phone: 914-365-8343
Fax: 914-365-3182
E-mail: chris@ldeo.columbia.edu

Elizabeth Pratson
Phone: 914-365-8313
Fax: 914-365-3182
E-mail: beth@ldeo.columbia.edu

Hole 973D: Natural Gamma Ray-Resistivity-Sonic Logging Data